Materials Today Bio 20 (2023) 100620

Contents lists available at ScienceDirect

Materials Today Bio

journal homepage: www.journals.elsevier.com/materials-today-bio

Nanocarriers of shRNA-Runx2 directed to collagen IV as a nanotherapeutic system to target calcific aortic valve disease

Geanina Voicu [a], Cristina Ana Mocanu [a], Florentina Safciuc [a], Maria Anghelache [a], Mariana Deleanu [b], Sergiu Cecoltan [a], Mariana Pinteala [c], Cristina Mariana Uritu [c,d], Ionel Droc [e], Maya Simionescu [a], Ileana Manduteanu [a], Manuela Calin [a,*]

[a] "Medical and Pharmaceutical Bionanotechnologies" Laboratory, Institute of Cellular Biology and Pathology "Nicolae Simionescu" of the Romanian Academy, 050568, Bucharest, Romania
[b] "Liquid and Gas Chromatography" Laboratory, Institute of Cellular Biology and Pathology "Nicolae Simionescu" of the Romanian Academy, 050568, Bucharest, Romania
[c] Centre of Advanced Research in Bionanoconjugates and Biopolymers, "Petru Poni" Institute of Macromolecular Chemistry, 700487, Iasi, Romania
[d] Advanced Centre for Research-Development in Experimental Medicine, Grigore T. Popa University of Medicine and Pharmacy of Iasi, 700115, Iasi, Romania
[e] Central Military Hospital "Dr. Carol Davila", Cardiovascular Surgery Clinic, Bucharest, Romania

ARTICLE INFO

Keywords:
Calcific aortic valve disease
Collagen IV
Lipopolyplexes
Runx2
shRNA
Valvular interstitial cells

ABSTRACT

Runx2 is a key transcription factor involved in valvular interstitial cells (VIC) osteodifferentiation, a process actively entwined with the calcific aortic valve disease (CAVD). We hypothesize that a strategy intended to silence Runx2 could be a valuable novel therapeutic option for CAVD. To this intent, we aimed at (i) developing targeted nanoparticles for efficient delivery of short hairpin (sh)RNA sequences specific for Runx2 to the aortic valve employing a relevant mouse model for CAVD and (ii) investigate their therapeutic potential in osteoblast-differentiated VIC (oVIC) cultivated into a 3D scaffold. Since collagen IV was used as a target, a peptide that binds specifically to collagen IV (Cp) was conjugated to the surface of lipopolyplexes encapsulating shRNA-Runx2 (Cp-LPP/shRunx2). The results showed that Cp-LPP/shRunx2 were (i) cytocompatible; (ii) efficiently taken up by 3D-cultured oVIC; (iii) diminished the osteodifferentiation of human VIC (cultured in a 3D hydrogel-derived from native aortic root) by reducing osteogenic molecules expression, alkaline phosphatase activity, and calcium concentration; and (iv) were recruited in aortic valve leaflets in a murine model of atherosclerosis. Taken together, these data recommend Cp-LPP/shRunx2 as a novel targeted nanotherapy to block the progression of CAVD, with a good perspective to be introduced in practical use.

1. Introduction

Calcific aortic valve disease (CAVD) is a chronic, multi-factorial disorder characterized by fibrosis and active valve leaflets calcification [1] causing narrowing of the aortic annulus that affects the valvular motion with further complications, such as cardiac hypertrophy and heart failure [2]. It occurs mainly in the elderly and in patients with diabetes, obesity, or renal disease posing significant health problems in the absence of any efficient pharmacological treatment. Clinical studies indicate an association of diabetes with an increased risk of developing aortic stenosis (AS) [3–5]and diabetes may be considered a predicting factor for the development of AS [6–8]. A high degree of calcification in the aortic valves of patients with diabetes mellitus compared to non-diabetic patients was demonstrated by histological analysis [9]. At present, the only efficacious interventions are surgical replacement or transcatheter aortic valve implantation (TAVI), yet with many inevitable complications [10,11].

The pathological processes that underlie the progression of CAVD include valvular endothelial cells (VEC) dysfunction, chronic inflammation, lipid deposition, extracellular matrix remodeling, neovascularization, and ectopic calcification mainly due to valvular interstitial cells (VIC) osteodifferentiation [12]. Pathological stimuli, such as atherogenic factors (e.g. lipid oxidation products, inflammatory mediators, hyperglycemia) and increased mechanical stress, induce inflammatory and remodeling molecules expression in VIC [13] and their

* Corresponding author. "Medical and Pharmaceutical Bionanotechnologies" Laboratory, Institute of Cellular Biology and Pathology "Nicolae Simionescu" of the Romanian Academy, 050568, Bucharest, Romania.
E-mail address: manuela.calin@icbp.ro (M. Calin).

https://doi.org/10.1016/j.mtbio.2023.100620
Received 9 February 2023; Received in revised form 22 March 2023; Accepted 27 March 2023
Available online xxxx

differentiation into osteoblast-like cells expressing osteogenic proteins, notably Runt-related transcription factor 2 (Runx2)/Core-binding factor 1 (Cbfa1), bone morphogenic proteins (BMP), osteopontin (OSP), osteocalcin (OSC) and alkaline phosphatase (ALP) [14,15].

The transcription factor Runx2, besides its critical role in bone formation, is also a key molecule involved in valvular calcification, inducing the expression of osteoblast markers in VIC [16,17]. Thus, an attractive strategy for CAVD treatment is to downregulate Runx2 expression using RNA interference (RNAi) for blocking the differentiation of human aortic VIC into osteoblast-like cells (oVIC). In previous studies, we provided evidence that specially designed nanoparticles carrying short hairpin (sh) RNA specific for Runx2 reduce the osteodifferentiation of human aortic VIC by downregulating the expression of Runx2 and other osteogenic proteins (OSP, BSP, BMP2) [18,19]. Recently, we reported the design and synthesis of cyto- and hemocompatible targeted nanocarriers, namely lipopolyplexes consisting of lipid bilayer-encapsulated fullerene (C60)-polyethyleneimine (PEI)/shRunx2 polyplexes, functionalized with a peptide with high affinity for the overexpressed vascular cell adhesion molecule 1 (VCAM-1) for specific delivery to oVIC [19].

In the present study, we found an increased expression of collagen IV in 3D-cultured VIC exposed to osteogenic media (compared to native VIC) as well as in the aortic valve leaflets of diabetic/hyperlipidemic ApoE-deficient mice. This fact proposes collagen IV as an appropriate target for the specific delivery of lipopolyplexes to the aortic valve. Thus, we aimed to characterize the collagen IV-targeted lipopolyplexes for Runx2 silencing in cultured oVIC seeded into a three-dimensional (3D) system (mimicking that of the native aortic valve) and *in vivo*, following their localization into the diseased aortic valve in a mouse model.

We report here the preparation and characterization of collagen IV-targeted lipopolyplexes surfaced with a collagen IV-binding peptide (Cp-LPP/shRunx2). The collagen IV-targeted lipopolyplexes specifically accumulate into the heart, aorta, and aortic valve after intravenous (i.v.) administration in a murine model of atherosclerosis complicated with diabetes (i.e. diabetic/hyperlipidemic ApoE-deficient mice). Importantly Cp-LPP/shRunx2 mitigate the osteoblast differentiation of VIC, thus being a novel targeted nanotherapy to block the progression of CAVD.

2. Materials and methods

2.1. Reagents

The commercial sources of the main reagents and consumables used in this study were as follows: Dulbecco's modified Eagle's medium (DMEM), Runx2 MISSION shRNA Plasmid DNA (MISSION Runx2 shRNA plasmid DNA, cat. no. SHCLND-NM_004348) sequence specific for human Runx2, namely the clone TRCN0000013653 from The RNAi Consortium (TRC) Version 1 library, GenElute-Plasmid Midiprep kit, fish gelatin and liberase DH were from SIGMA-Aldrich (Merck KGaA, Darmstadt, Germany); fetal bovine serum (FBS), penicillin and streptomycin from Gibco (ThermoFisher Scientific, Waltham, MA, USA); cell culture dishes were from TPP® (Trasadingen, Switzerland); Quant-iT™ PicoGreen® dsDNA kit and Tris (2-carboxyethyl) phosphine (TCEP), rabbit antibody anti-collagen IV A2, donkey anti-rabbit IgG conjugated with Alexa Fluor 594, secondary antibody goat anti-rabbit IgG conjugated with horseradish peroxidase (HRP), ProLong Gold Antifade Mountant with 4′,6-diamidino-2-phenylindole (DAPI), Tween and SuperSignal West Dura chemiluminescent substrate were from ThermoFisher Scientific (Waltham, MA, USA); Cy3-labeled plasmid was purchased from Mirus Bio (Madison, WI, USA); 1,2-dioleoyl-sn-glycero-3-phospho-(1′-rac-glycerol) (sodium salt) (DOPG), 1-palmitoyl-2-oleoyl-*glycero*-3-phosphocholine (POPC), 1,2-distearoyl-sn-glycero-3-phosphoethanolamine-*N*-[methoxy(polyethylene glycol)-2000] (ammonium salt) 1,2-distearoyl-sn-glycero-3-phosphoethanolamine-*N*-[Maleimide(PolyethyleneGlycol)2000] (Ammonium salt) (Mal-PEG-DSPE), and 1,2-dipalmitoyl-sn-glycero-3-phosphoethanolamine-*N*-(lissamine rhodamine B sulfonyl) (ammonium salt) (Rhodamine B-DSPE) were from Avanti Polar Lipids (Alabaster, AL, USA); collagen IV recognition peptide and the peptide with scrambled sequence of aminoacids were synthesized by GeneCust (Dudelange, Luxembourg); SpectraPor dialysis membrane (cut-off 100–500 Da) was from Spectrum Labs (Spectrum Europe BV, Breda, The Netherlands); 100 kDa cut-off Amicon centrifugal filter columns were from Millipore (Billerica, MA, USA); ToxiLight™ Cytotoxicity BioAssay Kit was from Lonza (Basel, Switzerland); TBS Blotto A was from Santa Cruz (Dallas, TX, USA); SensoLyte pNPP Alkaline Phosphatase Assay Kit was from AnaSpec (CA, USA), Calcium Colorimetric Assay kit was purchased from Biovision (CA, USA) and HPLC grade solvents were from Merck (Kenilworth, NJ, USA). Deionized water (18.2 MΩ/cm) was obtained in-house using a Milli-Q system from Millipore (Watford, UK).

2.2. Preparation of lipid-coated C60-PEI/shRNA polyplexes (lipopolyplexes)

The lipopolyplexes (LPP) were prepared as previously described [19], by employing a reverse-phase evaporation technique. For the synthesis of LPP, MISSION® pLKO.1-puro Non-Mammalian shRNA Control Plasmid DNA (shCtr) or MISSION®shRNA Plasmid DNA targeting human Runx2 gene (shRunx2) (Sigma-Aldrich cat. no. SHCLND-NM_004348, clone TRCN0000013653), validated by us as having a high silencing effect in previous studies [18], were used. The amplification of plasmids was done in *Escherichia coli* host strain DH5α and the isolation was performed using GenElute-Plasmid Midiprep kit (Sigma-Aldrich, Germany). First, the C60-PEI/shRNA polyplexes were formed from conjugated fullerene (C60)-polyethyleneimine (PEI) and shRNA plasmids at an N/P ratio (ratio of nitrogen atoms in C60-PEI to phosphorus atoms in DNA) of 25 as previously reported [20]. C60-PEI and shRNA were diluted in the same volume of 2 × HB buffer (20 mM HEPES, 10% D-glucose, pH = 7.4) to achieve an appropriate concentration, and brought up to the final volume of 1000 μL with HB buffer (10 mM HEPES, 5% D-glucose, pH = 7.4). Next, the preformed cationic polyplexes were mixed with 3 mM anionic phospholipid DOPG dissolved in chloroform/methanol in a ratio of 2:1 (v/v) to form reverse micelles. After incubation for 30 min at room temperature and the addition of 3 mL of chloroform and distilled water (1:1, v/v), the mix was centrifuged at 830×*g* for 7 min. The aqueous phase was removed and the organic phase was mixed with 6.7 mM POPC, 0.1 mM Mal-PEG-DSPE, and 0.1 mM PEG-DSPE diluted in chloroform. For *in vitro* uptake studies, the lipopolyplexes were obtained using a fluorescent Cy3-labeled plasmid instead of the plasmids containing shRNA sequences. For *ex vivo* imaging studies on mice, the lipopolyplexes were fluorescently labeled with 0.1 mM Rhodamine B-DSPE added from an ethanol stock solution, after LPP preparation. Also, to study the transfection efficiency, the lipopolyplexes were obtained using the pEYFP-C1 plasmid (~4700 base pairs, Clontech Laboratories Inc.) encoding the yellow variant of green fluorescent protein. The mix containing inverted micelles encapsulating polyplexes and lipids was vortexed, sonicated for 1 min, and subjected to chloroform evaporation under vacuum on a rotary evaporator (Laborota 4000, Heidolph, Schwabach, Germany), at 37 °C. The lipid-enveloped C60-PEI/shRNA polyplexes (lipopolyplexes) deposited as a lipidic film were rehydrated overnight at 4 °C and extruded through 200 nm and 100 nm polycarbonate membranes using a hand extruder from Avanti Polar Lipids (Alabaster, AL, USA), obtaining lipopolyplexes encapsulating shRunx2 (LPP/shRunx2) or shCtr (LPP/shCtr) with a homogenous size distribution.

2.3. Coupling of collagen IV binding-peptide to the lipopolyplexes surface

The lipopolyplexes were coupled with collagen IV-binding peptide (NH2-KLWVLPKGGGC-COOH) or with a scrambled sequence of amino acids (NH2-LKPWLKVGGGC-COOH), containing a cysteine residue in the carboxy-terminal domain resulting in collagen IV-targeted lipopolyplexes (Cp-LPP) and non-targeted lipopolyplexes (S-LPP). The collagen IV binding-peptide, having the sequence NH2-KLWVLPKGGGC-COOH,

contains the heptapeptide amino acids sequence "KLWVLPK" identified by phage display [21] to bind with high affinity to collagen IV. Before coupling, the peptides were reduced with tris (2-carboxyethyl) phosphine (TCEP), for 2 h at room temperature, to break the disulfide bonds. Overnight dialysis at 4 °C against coupling buffer (10 mM Na_2HPO_4, 10 mM NaH_2PO_4, 2 mM EDTA, 30 mM NaCl, pH = 6.7), using membranes of 500–1000 Da, was performed to remove the excess TCEP. The reduced peptides were added to the LPP solution and incubated overnight at 4 °C to form the bonds between the maleimide group at the distal end of the phospholipid Mal-PEG-DSPE inserted into liposomes' bilayer and cysteine from the carboxy-terminal end of peptides. An excess L-cysteine (1 mM) was incubated with LPP for 30 min at room temperature to saturate the non-reacted maleimide. The unbound peptides were removed by filtration using Amicon centrifugal filter units of 100 kDa. Ultra-High-Performance Liquid Chromatography (UHPLC) was used to indirectly measure the concentration of peptides coupled to the surface of LPP by quantifying the uncoupled peptides, as previously described [22]. The concentration of the shRNA plasmids encapsulated into the lipopolyplexes was determined using the Quant-iT™ PicoGreen® dsDNA kit (ThermoFisher Scientific, cat. no. R11490) as described [19].

2.4. Characterization of lipopolyplexes

The hydrodynamic diameter and the Zeta potential of LPP were measured in water (1:1000 dilution) by dynamic light scattering (DLS) and electrophoretic light scattering (ELS), respectively, on a Zetasizer Nano ZS instrument (ZEN 3600, Malvern Instruments, Malvern, UK). The Zeta potential was measured using a Zeta dip cell (ZEN 1002) immersed in the sample. For each sample, three records of an average of 13 measurements were acquired for size and Zeta potential determinations. The physical stability of LPP stored at 4 °C for one month was checked by periodical measurement of size and Zeta potential at 1, 2, 3, and 4 weeks. The results were analyzed using the built-in Zetasizer Software 7.12 (Malvern Instruments, Malvern, UK).

2.5. In vitro studies

2.5.1. Isolation and culture of human valvular interstitial cells

Primary valvular interstitial cells (VIC) originated from the non-calcified portions of human aortic valve leaflets obtained from a patient who underwent aortic valve replacement surgery at Central Military Hospital "Dr. Carol Davila", Bucharest, as previously described [18]. The patient gave written informed consent and his anonymity and privacy rights were respected. The surgery was carried out according to the principles outlined in the Declaration of Helsinki for experiments involving human samples [23]. All the studies performed on these cells were approved by the Ethics Committee of the Institute of Cellular Biology and Pathology "Nicolae Simionescu".

To investigate whether the developed nanocarriers also function as vehicles for shRNA delivery to osteodifferentiated VIC in a more complex environment, mimicking the composition of the aortic valve, we performed comparative experiments in 2D versus 3D cell culture systems.

Two-dimensional (2D) cell culture. Cultured VIC, between passages three to eight, were grown to confluence on 1% gelatin-coated plates in DMEM medium containing 5.5 mM glucose, supplemented with 10% fetal bovine serum, 50 μg/mL neomycin, 100 UI/mL penicillin, and 100 μg/mL streptomycin, at 37 °C, in a humidified incubator with 5% CO_2.

Three-dimensional (3D) cell culture. A 3D-hydrogel consisting of the extracellular matrix of the aortic root, previously proved as a suitable platform, was used to simulate the natural situation of VIC embedded in an origin tissue-like environment [24]. The 3D cell culture model was obtained by incorporation of VIC in a hydrogel derived from the cell-free native aortic root (ARdH) obtained and characterized as described elsewhere [24]. The ARdH is a physiologically relevant matrix environment for VIC culture being composed mainly of type I collagen similar to aortic valve fibrosa, where calcification is mainly observed. This 3D scaffold maintains a quiescent fibroblast-like phenotype of VIC and allows VIC osteodifferentiation when exposed to pathological conditions [24]. Before cell incorporation, the ARdH was neutralized with NaOH to a final concentration of 10 mM, buffered with 10 × phosphate buffer saline (PBS) to 1 × concentration, and homogenized by pipetting. The hydrogel was centrifuged at 3000×*g* for 15 min at 4 °C to remove the air bubbles. The VIC were seeded at a density of 0.3×10^6 cells/mL hydrogel by carefully mixing 50 μL of cell suspension in the hydrogel. Then, the hydrogel-cells mixture was divided into 100 μL volume in low adhesion 48-wells for obtaining the 3D constructs with a diameter of 8 mm and a thickness of 1 mm. After 2 h of incubation at 37 °C to allow gelling, a complete DMEM culture medium was added to each well.

For the experiments, VIC were cultured either in 2D or 3D in different conditions, in a medium containing: (i) normal glucose (NM), 5 mM glucose concentration, (ii) high glucose (HG), 25 mM glucose concentration, (iii) osteogenic medium (OM), consisting in normal, 5.5 mM glucose and osteogenic factors (50 μg/mL ascorbic acid, 10 mM β-glycerophosphate, 10 nM dexamethasone) and (iv) medium containing high, 25 mM glucose and osteogenic factors (HGOM).

2.5.2. Collagen IV expression in VIC seeded in 2D and 3D cell culture models

2.5.2.1. Collagen IV protein expression in VIC cultivated on 2D support. ***Western blot assay.*** Timely collagen IV protein expression in VIC seeded on 2D support was assessed by Western blot assay. VIC were seeded at 2×10^5 cells/well density in a 6-well plate and incubated in NM, HG, OM, or HGOM medium. The medium was refreshed every two days. After 2, 7, 14, or 21 days the cells were lysed in S × 2 Laemmli buffer, and the protein concentrations were determined by Amido Black assay. Then, 30 μg/lane of cell protein extracts were separated in 10% SDS-PAGE gels and transferred onto a nitrocellulose membrane. The blots were probed overnight with primary antibody rabbit anti-collagen IV (1:500) or rabbit anti-β actin (1:1000). After washing, the blots were incubated with secondary antibody goat anti-rabbit IgG conjugated with horseradish peroxidase (HRP, 1:1000), for 1 h at room temperature, washed again and, then, incubated with SuperSignal West Dura chemiluminescent substrate. The protein bands were visualized using a G: Box Chemi XX6 System analyzer (Labgene Scientific, Châtel Saint-Denis, Switzerland) and were quantified by densitometry using ImageJ software version 1.8.0 developed at the National Institutes of Health (NIH), USA. The collagen IV protein expression was normalized to β-actin and estimated as fold change versus expression on day 2. The data were expressed as mean ± S.D. (standard deviation) of two experiments performed in duplicates.

Immunofluorescence. After seeding of VIC on 1% gelatin-coated glass cover slides placed in 24-well plates (2.5×10^4 cells/well), the cells were exposed to NM and HGOM medium for 2, 7, and 14 days to investigate the expression of collagen IV by fluorescence microscopy. At the end of the incubation period, the collagen IV expression was assessed by immunofluorescence. The cells were washed with cold PBS, fixed in 100% methanol for 6 min at 4 °C, and blocked in 1% bovine serum albumin (BSA) in PBS for 1 h at room temperature. After blocking, the cells were incubated with primary antibody rabbit anti-collagen IV (cat. no. PA5-79058, ThermoFisher Scientific, 1:250 dilution), overnight at 4 °C. The next day, after washing with PBS, VIC were incubated with the secondary Alexa Fluor 594-conjugated donkey anti-rabbit antibody (cat. no. A-21207, ThermoFisher Scientific, 1:1000 dilution) for 1 h at room temperature. Next, the cover slides were washed with PBS and distilled water and mounted with ProLong Gold Antifade Mountant with 4′,6-diamidino-2-phenylindole (DAPI). The collagen IV expression was analyzed by fluorescence microscopy using an Olympus IX81 microscope (Shinjuku City, Tokyo, Japan). Fluorescence images using tetramethylrhodamine (TRITC) (red) and DAPI (blue) filters were acquired using CellSense Dimensions software. For each captured image, the mean fluorescence intensity of the red histogram (collagen IV) was normalized

to the number of nuclei. Five fields per sample were used for analysis using ImageJ software version 1.8.0 (NIH, USA).

2.5.2.2. Collagen IV protein expression in VIC seeded in the 3D hydrogel. ***Immunofluorescence.*** The 3D cell model was obtained, as mentioned above, in 2.5.1. section, the VIC being seeded at a density of 0.3×10^6 cells/mL of the hydrogel. The next day, the 3D seeded VIC were incubated in NM or HGOM culture medium for 7 days, with a refresh every two days. At the end of the incubation period, the samples were cryoprotected following the steps described in Ref. [24]. The 3D constructs were washed with PBS and then fixed in 4% paraformaldehyde for 30 min at 37 °C, followed by successive washing with PBS, and 5%, 10%, and 20% glycerol solution. After washing in 3% sucrose, the constructs were embedded in Optimal cutting temperature compound (OCT) (cat. no. Neg-50, ThermoFisher Scientific) and sectioned on a Leica CM1850 cryomicrotome (Leica Biosystems, Nussloch Gmbh, Germania). Four sections of 5 μm in thickness were placed on a glass microscope slide covered with poly-L-lysine. To visualize the collagen IV expression, the cryosections were washed with warm PBS and blocked in TBS Blotto A (cat. no. SC-2333, Santa Cruz) with 1% BSA, 0.2% Tween (cat. no. 85113, ThermoFisher Scientific) and 1% cold fish gelatin (cat. no. G7041, Sigma) for 1 h at room temperature, followed by the overnight incubation at 4 °C with primary anti-collagen IV antibody (cat. no. PA5-79058, ThermoFisher Scientific) at 1:250 dilution in PBS with 3% BSA. The next day, the slides were washed with PBS and incubated with Alexa Fluor 594-conjugated secondary anti-rabbit antibody (cat. no. A-21207, ThermoFisher Scientific) 1:1000 dilution in PBS with 1% BSA and 0.3% TritonX-100, for 1 h at room temperature. After washing in PBS and distilled water, the slides were mounted in ProLong Gold Antifade Mountant with DAPI. Images were acquired using an Olympus IX81 microscope equipped with TRITC (red) and DAPI (blue) fluorescent filters and processed using ImageJ software. The collagen IV levels for each condition were expressed as mean fluorescence intensity calculated from 3 images per section.

2.5.3. Evaluation of the cytotoxicity of lipopolyplexes

The potential cytotoxicity of lipopolyplexes on VIC cultured in 2D and 3D models was evaluated using the ToxiLight™ Cytotoxicity BioAssay Kit (cat. no. LT17-217, Lonza Bioscience, Basel, Switzerland) [25]. The assay method measures the adenylate kinase (AK) released in the culture medium after cell' membrane degradation. The 2D culture was established by seeding VIC in a 24-well plate at a density of 5×10^4 cells/well, while the 3D culture was obtained by seeding the aortic root-derived hydrogel with VIC as mentioned above (0.3×10^6 cells/mL hydrogel in a 48-well plate). Twenty-four hours after seeding, the cells were incubated in HGOM medium for 7 or 14 days, and, on the 5th and 12th day, they were transfected with lipopolyplexes targeted to collagen IV (Cp-LPP/shCtr), non-targeted (S-LPP/shCtr), and C60-PEI/shCtr polyplexes, at a concentration of one μg shRNA control plasmid (shCtr)/well. Forty-eight hours after the last transfection (on the 7th and 14th day), the medium was collected and used for AK determinations. The luminescence measurements were made at 1 s on a Mithras LB 940 Multimode Microplate Reader (Berthold Technologies GmbH & Co. KG, Oak Ridge, TN, USA). The data were normalized to values obtained on VIC grown in HGOM medium, considered 1, and were expressed as mean ± S.D. (standard deviation) of four experiments made in duplicates.

2.5.4. Cellular uptake of collagen IV-targeted lipopolyplexes by 2D- and 3D-cultured VIC

VIC were cultivated in 48-well plates (7×10^3 cells/well) (2D model) or in the 3D aortic root-derived hydrogel (0.3×10^6 cells/mL hydrogel). The next day, the cells were incubated in NM or HGOM medium for 5 days. Then, the medium was replaced with a fresh medium containing collagen IV-targeted or non-targeted lipopolyplexes, encapsulating polyplexes made of C60-PEI and a Cy3-labeled plasmid at N/P = 25 (Cp-LPP/Cy3 and S-LPP/Cy3, respectively), at a concentration of 0.3 μg DNA plasmid/well (for VIC cultured in 2D) and one μg Cy3 plasmid/3D-VIC seeded construct. The 2D cultured VIC were incubated with lipopolyplexes for 24 or 48 h, whereas the 3D cultured VIC were exposed to lipopolyplexes for 48 h. To investigate the specificity of Cp-LPP/Cy3 uptake in VIC, competitive studies were performed, in the presence of an excess of collagen IV binding peptide (25-fold higher concentration of Cp as compared to peptide coupled to the Cp-LPP/Cy3 surface). After examination using the Olympus IX81 fluorescence microscope equipped with a TRITC filter, the cells cultured on 2D supports were detached from the well and resuspended in FACS buffer (0.5% PFA in PBS) for flow cytometry determinations on a Gallios flow cytometer (Beckman Coulter, Brea, CA, USA) and the data were analyzed with Kaluza Flow analysis software (v.2.1). The 3D samples were processed for cryosectioning, as above mentioned in section 2.5.2.2. The sections were mounted in ProLong Gold Antifade Mountant with DAPI and visualized with the Olympus IX81 microscope. The microscopy images were processed using ImageJ software version 1.8.0 (NIH, U.S.A.) and the data were expressed as mean fluorescence intensity normalized to the number of cell nuclei from at least five fields per 2D samples and as mean fluorescence intensity for 3D samples.

2.5.5. Transfection efficiency of collagen IV-targeted lipopolyplexes in 2D- and 3D-cultured VIC

VIC seeded at a density of 1×10^4 cells/well in a 24-well plate for the 2D model and at 0.3×10^6 cells/mL hydrogel for the 3D model were maintained in HGOM medium for 5 days and incubated for 48 h with Cp-LPP/pEYFP or non-targeted S-LPP/pEYFP, at a concentration of one μg pEYFP plasmid/probe. At the end of the incubation period, the cells cultured on 2D supports were examined using an Olympus IX81 fluorescence microscope. After detachment from the well, the resuspended cells in FACS buffer (0.5% PFA in PBS) were examined by flow cytometry on a Gallios flow cytometer (Beckman Coulter, Brea, CA, USA) and the data were analyzed with Kaluza Flow analysis software (v.2.1). The 3D samples were processed for cryosectioning, as described above in section 2.5.2.2. After washing with warm PBS, the sections were mounted in ProLong Gold Antifade Mountant with DAPI and visualized at an Olympus IX81 microscope. The microscopy images were processed using ImageJ software version 1.8.0 (NIH, U.S.A.) and the data were expressed as mean fluorescence intensity normalized to the number of cell nuclei for the 2D samples and as mean fluorescence intensity for the 3D samples from at least five fields per probe.

2.5.6. Transfection of 2D- and 3D-cultured VIC with Cp-LPP/shRunx2 lipopolyplexes

VIC seeded on the 2D support (48-well plates, 7×10^3 cells/well) and in the 3D hydrogels (0.3×10^6 cells/mL hydrogel) were exposed for 7 or 14 days to NM or HGOM medium. On the 5th and 12th day of culture, the cells were transfected with collagen IV-targeted lipopolyplexes (Cp-LPP) or non-targeted lipopolyplexes (S-LPP) encapsulating the shRNA plasmid with specificity for human gene Runx2. Also, the C60-PEI/shRunx2 polyplexes were used for transfection. As negative controls, pLKO.1-puro non-mammalian shRNA control plasmid DNA (shCtr) was used to obtain Cp-LPP/shCtr and S-LPP/shCtr lipopolyplexes. The plasmid DNA concentration employed was one μg shRunx2 or shCtr plasmid DNA/well.

2.5.7. Assessment of osteogenic gene expression in VIC after transfection with Cp-LPP/shRunx2 lipopolyplexes

Forty-eight hours after the last transfection (on the 7th and 14th day), total cellular RNA was isolated using TRIzol™ reagent according to the manufacturer's protocol. After determination of RNA concentration with a Spectrophotometer NanoDrop 1000 (ThermoFisher Scientific, Waltham, MA, USA), one μg of total RNA was reverse transcribed using M-MLV (Moloney murine leukemia virus) reverse transcriptase (Invitrogen, ThermoFisher Scientific, Waltham, MA, USA). Real-time PCR

Table 1
The sequences of primers for human genes used in Real-Time PCR analysis.

Gene	Forward	Reverse	Amplicon (bp)
Runx2	CCGCCTCAGTGATTTAGGGC	GGGTCTGTAATCTGACTCTGTCC	132
OSP	GAAGTTTCGCAGACCTGACAT	GTATGCACCATTCAACTCCTCG	91
BSP	GAACCTCGTGGGGACAATTAC	CATCATAGCCATCGTAGCCTTG	79
BMP2	ACTACCAGAAACGAGTGGGAA	GCATCTGTTCTCGGAAAACCT	113
ACTB	GACGAGGCCCAGAGCAAGAGAGG	CATGGCTGGGGTGTTGAAGGTCTC	231

experiments were performed in triplicates in a 96-well plate on a LightCycler 480 Real-Time PCR System from Roche (Basel, Switzerland), in the following optimized conditions: 2.5 mM $MgCl_2$, annealing at 60 °C, and extension at 72 °C. The Runx2, osteopontin (OSP), bone sialoprotein (BSP), and bone morphogenic protein 2 (BMP2) gene expressions were calculated using the $2^{-\Delta\Delta Ct}$ method as fold change relative to HGOM, and the results were normalized to the reference gene for ACTB (β-actin). The data were expressed as mean ± S.D. (standard deviation) of two experiments performed in triplicates. The primers used are presented in Table 1.

2.5.8. Quantification of alkaline phosphatase (ALP) activity in 3D-cultured VIC subjected to transfection with Cp-LPP/shRunx2 lipopolyplexes

To evaluate the effect of Runx2 down-regulation on osteogenic differentiation of VIC, we measured the alkaline phosphatase (ALP) activity in 3D cultured VIC exposed to HGOM for 7 or 14 days and transfected on the 5th and 12th day with Cp-LPP/shRunx2, S-LPP/shRunx2 lipopolyplexes, C60-PEI/shRunx2 polyplexes and LPP encapsulating control plasmid shCtr. After 48 h of transfection, the cells were isolated from the hydrogel with Liberase DH (cat. no. 05401054001, SIGMA-Aldrich) at 37 °C for 5 min. Then, the cells were enzymatically processed for ALP assay using SensoLyte pNPP Alkaline Phosphatase Assay Kit (AnaSpec, Inc. Fremont, CA, USA), as directed by the manufacturer [18]. Para-nitrophenyl phosphate (pNPP), used as a substrate, was incubated with the cell lysates for 30 min at room temperature, and the absorbance of the solution was read at 405 nm using a spectrophotometer TECAN Infinite M200Pro. The data were normalized to the total protein concentration from cell lysates and were expressed as mean ± S.D. (standard deviation) of two experiments performed in duplicates.

2.5.9. Quantification of calcium content in 3D-cultured VIC after exposure to Cp-LPP/shRunx2 lipopolyplexes

Determination of calcium concentration. VIC-laden hydrogel constructs were exposed for 7 or 14 days to HGOM medium and transfected on the 5th and 12th day with Cp-LPP/shRunx2, S-LPP/shRunx2, and C60-PEI/shRunx2 polyplexes. The Cp-LPP/shCtr and S-LPP/shCtr lipopolyplexes were used as negative controls. Forty-eight hours after transfection, the cells were released from the 3D constructs with Liberase DH (cat. no. 05401054001, SIGMA-Aldrich) and the calcium concentration was measured in the cell lysates using the Calcium Colorimetric Assay kit (Biovision, Inc. Fremont, CA, USA) by measuring the absorbance at 575 nm using a spectrophotometer TECAN Infinite M200Pro (Tecan Group Ltd., Männedorf, Switzerland). The data were normalized to total protein concentration and expressed as mean ± S.D. (standard deviation) of two experiments performed in duplicates.

Cytochemical staining of calcium deposits. 3D-cultured VIC were exposed to HGOM for 12 days and then transfected with different types of lipopolyplexes. After 48 h, the cells were stained with Alizarin Red S (SIGMA-Aldrich), as described elsewhere [26]. The Alizarin Red S sodium salt binds the calcium crystals formed in the cells or the extracellular matrix. After washing with PBS, the VIC-laden 3D constructs were fixed in 4% paraformaldehyde (90 min at 37 °C) and then incubated with 2% (40 nmol/L) Alizarin Red solution, pH = 4.1–4.3, for 30 min, protected from light. After a visual investigation by optic microscopy, the dye was released from the hydrogels with 10% acetic acid (30 min) and the neutralization was achieved with 10% ammonium hydroxide. The absorbance was measured at 405 nm with a spectrophotometer TECAN Infinite M200Pro. The data were expressed as mean ± S.D. (standard deviation) of two experiments performed in triplicates.

2.6. In vivo studies

2.6.1. Animal model

Recently, we described an experimental murine model of diabetes/atherosclerosis as suitable for early molecular and functional changes in aortic heart valves [27]. Thus, we used this model for testing the collagen IV-targeted nanocarriers of shRunx2 since it has the advantage of expressing, in the aortic valve, significantly increased levels of inflammation- and osteogenesis-associated proteins at shorter periods [27] compared with other animal models [28].

Twelve weeks old male ApoE-deficient and C57BL/6 mice from Taconic Biosciences, bred in our specific-pathogen-free (SPS) facility, were kept on a 12 h light/dark cycle, with water and standard chow diet *ad libitum*. To induce diabetes and accelerate the pathological modification in the aortic valve, the animals were given streptozotocin (STZ) (55 mg/kg body weight), in a total volume of 150 μL 0.9% NaCl by intraperitoneal injection, for 5 consecutive days. On the 5th day of STZ injection a high-fat diet (HFD), consisting of a standard chow diet with 15% butter (82% fat) and 1% cholesterol, was started.

The experiments were approved by the Ethics Committee of the Institute of Cellular Biology and Pathology "Nicolae Simionescu" and by the National Sanitary Veterinary and Food Safety Authority authorization no. 448/April 02, 2019 and were performed in accordance with the Romanian Law no. 43/2014 (Official Monitor, Part I nr. 326 pages 2–4), which transposes the EU directive 2010/63/EU on the protection of animals used for scientific purposes.

2.6.2. Collagen IV expression in the aortic valve of a murine model of atherosclerosis

Seven days after the HFD was started, the diabetic/hyperlipidemic $ApoE^{-/-}$ mice (n = 3) were anesthetized with ketamine/xylazine, the blood was drawn via cardiac puncture and the vasculature was rinsed by injecting cold PBS in the left ventricle using a peristaltic pump. Explanted aortic root specimens were embedded in the OCT compound for cryosectioning using a Leica CM1850 cryomicrotome (Leica Biosystems, Nussloch Gmbh, Germany). Three sections (5 μm thick) were harvested per slide, and 10 slides were prepared per mouse. The slides were rinsed with PBS for 30 min and then, incubated with primary antibody rabbit anti-human/mouse collagen IV (cat. no. PA5-79058, ThermoFisher Scientific,1:250), overnight at 4 °C. The next day, after washing with PBS, the sections were incubated for 1 h at room temperature with the secondary donkey anti-rabbit antibody conjugated with Alexa Fluor 594 (cat. no. A-21207, ThermoFisher Scientific) at a 1:1000 dilution. Finally, after washing with PBS and distilled water, the slides were mounted in ProLong Gold Antifade Mountant with DAPI and investigated using an Olympus IX81 fluorescence microscope. The image processing was performed using the ImageJ program version 1.8.0 (NIH, U.S.A.).

2.6.3. Biodistribution of collagen IV-targeted lipopolyplexes by ex vivo imaging in experimental diabetic/hyperlipidemic mice

Twelve weeks old ApoE-deficient mice were injected with STZ for 5 days and had been on an HFD for one week before the i.v. injection of

fluorescently-labeled lipopolyplexes with Rhodamine B-DSPE (1 mol%). The collagen IV-targeted (Cp-LPP/shCtr) or non-targeted lipopolyplexes (S-LPP/shCtr) encapsulating polyplexes C60-PEI/shCtr were administered retro-orbitally, under anesthesia, at a dose of 10 μmols lipids/1.5 mg shRNA control plasmid per kg body weight (150 μL/mouse) (n = 4 for each lipopolyplexes formulation). A mouse receiving sterile PBS was used as a control for fluorescence background. Ninety minutes after lipopolyplexes administration, the mice were sacrificed, exsanguinated, and perfused with PBS via the left ventricle to wash the vasculature. The brain, lungs, heart and aorta, liver, spleen, and kidneys were harvested and the Rhodamine B fluorescence was visualized with an IVIS Imaging System 200 (Caliper Life Sciences, Waltham, Massachusetts, USA) using λex = 535 nm and λem = 620 nm. Separately, the aortic roots were excised and visualized with the IVIS Imaging System at the same wavelengths. Quantification of the fluorescent radiant efficiency [(radiance of the fluorescent emission per incident excitation intensity (p/s/cm^2/sr)/(μW/cm^2)] was performed with the region of interest (ROI) tool of Living Image 4.3.1 software.

Moreover, the localization of Cp-LPP/shCtr and S-LPP/shCtr lipopolyplexes labeled with Rhodamine B-DSPE was evaluated on valve cryosections obtained as above. The slides mounted in ProLong Gold Antifade Mountant with DAPI were visualized with an Olympus IX81 fluorescence microscope.

2.6.4. Assessment of liver and renal function after lipopolyplexes administration to diabetic/hyperlipidemic mice

The safety of lipopolyplexes administration was evaluated in plasma collected from healthy C57BL/6 mice fed with a standard chow diet and water *ad libitum*. The animals were i.v. injected with 10 μmols lipids/1.5 mg shCtr/kg body weight (100 μL LPP/shCtr per mouse) (n = 3 for each LPP formulation: Cp-LPP/shCtr, S-LPP/shCtr). Mice injected with PBS (n = 3) were used as a control. Twenty-four hours after lipopolyplexes administration, the blood was collected on 5 mM EDTA via open heart puncture and centrifuged at 2000 rpm for 10 min at 4 °C to obtain the plasma. The hepatic and renal biochemical parameters were quantified in plasma using ELISA assay kits: transaminases aspartate aminotransferase (AST; cat. no. D94610), alanine aminotransferase (ALT; cat. no. D94620), plasma urea (BUN; cat. no. 402999), creatinine (cat. no. D95595), from DiaLab (Neudorf, Austria) and alkaline phosphatase (ALP; cat. no. AF2910) from R&D Systems (Minneapolis, USA), following the manufacturer's instructions. The absorbance of each probe was measured at the recommended wavelengths using a spectrophotometer (TECAN Infinite M200Pro, Tecan Group Ltd., Männedorf, Switzerland).

2.7. Statistics

The data were expressed as mean ± standard deviation (S.D.) for experiments performed in triplicate. Statistical analyses were performed using GraphPad™ Prism software version 9.2.0 (GraphPad Software, La Jolla, CA). The statistical differences were calculated with an unpaired two-tailed *t*-test for comparing two groups or one-way ANOVA with multiple comparisons posthoc Tukey test for comparing three or more groups. Statistically significance of differences: one symbol (e.g. *, $^{\#}$, $^{\&}$) $p < 0.05$, two symbols (e.g. **, $^{\#\#}$, $^{\&\&}$) $p < 0.01$, three symbols (e.g. ***, $^{\#\#\#}$, $^{\&\&\&}$) $p < 0.001$.

3. Results

3.1. Characterization of collagen IV-targeted lipopolyplexes

The average hydrodynamic diameter of lipopolyplexes as measured by DLS was ~200 nm immediately after synthesis (time 0) (Fig. 1 A-a) and the polydispersity index (PDI) was between 0.2 and 0.3, indicating a homogenous population of nanoparticles. The ELS measurements showed that both types of lipopolyplexes were stable negatively charged nanoparticles with an average Zeta potential of ~ −35 mV (Fig. 1 A-b), indicating the complete encapsulation of the positively C60-PEI-based polyplexes by the external negatively charged lipid membrane. The stability of lipopolyplexes was determined at different time intervals, up to 4 weeks, by measuring the size and the Zeta potential of lipopolyplexes stored at 4 °C. There were no significant changes in size and Zeta potential, the lipopolyplexes being stable for the investigated period. The HPLC measurements determined ~7.2 μg collagen IV peptide per μmol lipid coupled to the surface of lipopolyplexes. The quantification of shRNA plasmid loaded into lipopolyplexes using Quant-iT PicoGreen reagent showed about 9.8 μg shRNA plasmid DNA entrapped per μmol lipid.

3.2. Collagen IV-targeted lipopolyplexes are cytocompatible

The cytotoxicity of lipopolyplexes was assessed for osteodifferentiated VIC (cultured in 2D and 3D culture models) by ToxiLight assay at 48 h after a single or a double transfection (performed on days 5 and 12 of the HGOM activation period), by measuring the AK released from damaged cells. The data were normalized and presented as fold change of cells exposed to HGOM for 7 or 14 days, in the absence of lipopolyplexes, considered 1. Both Cp-LPP/shCtr and S-LPP/shCtr lipopolyplexes and C60-PEI/shCtr polyplexes were found cytocompatible with osteodifferentiated VIC cultured in the 2D or 3D models (Fig. 1 B-a, b) as the values for AK release were smaller than 1. The absence of the cytotoxic effect of lipopolyplexes after a single or a double transfection of oVIC indicated that they were a safe carrier for the delivery of shRNA plasmid to cells.

3.3. High glucose concentration and osteogenic factors determine a time-dependent increase of collagen IV protein expression in osteodifferentiated VIC

2D-cultured VIC. The time-dependent protein expression of collagen IV in VIC cultured on 2D supports was evaluated after exposing the cells to different culture media (namely NM, HG, OM, and HGOM) for various intervals (2, 7, 14, or 21 days) by Western blot assay. We found that the expression of collagen IV in VIC grown in NM or HG medium did not vary significantly in time. However, a time-dependent increase for both OM and HGOM conditions was determined beginning with day 7 (Fig. 2 A). Two days of exposure to any medium did not induce significant variation in the collagen IV protein expression. A significant increase of ~2.7-fold was determined in VIC exposed to OM for 7 days compared to collagen IV expression at 2 days. At 14 and 21 days of exposure, the collagen IV expression increased by ~3.5-fold and ~4.8-fold, respectively, above the value determined on day 2. The increase at 14 and 21 days was significantly higher when compared with collagen IV levels in VIC incubated with OM for 7 days (by 1.3 and 1.7-fold change, respectively). Treatment of VIC with HGOM induced a significant increase in collagen IV levels on days 7, 14, and 21 by ~4.4, 4.7, and 6-fold, respectively, when normalized to that measured on day 2. These results suggest that at the investigated time intervals, high glucose concentration did not increase the collagen IV protein level. The synergistic action of high glucose concentration and osteogenic factors is necessary to induce a higher level of collagen IV protein expression than that expressed when exposed to a control culture medium.

These results were validated by the immunofluorescence studies that also showed the overexpression of collagen IV by VIC exposed to HGOM for 7 and 14 days (Fig. 2 B). The data showed that collagen IV expression remained constant in VIC grown in NM irrespective of the time of exposure.

3D-cultured VIC. Immunofluorescence staining was used to evaluate the collagen IV presence in VIC seeded on a 3D matrix and exposed to NM or HGOM medium for 7 days (Fig. 2 C). We found that in NM, the cells presented a scant amount of collagen IV, as depicted by calculating the mean fluorescence intensity by ImageJ software. In contrast, the mean fluorescence intensity of collagen IV in VIC exposed to HGOM (7 days) was significantly increased (~2.4-fold; $p < 0.001$) compared to the value

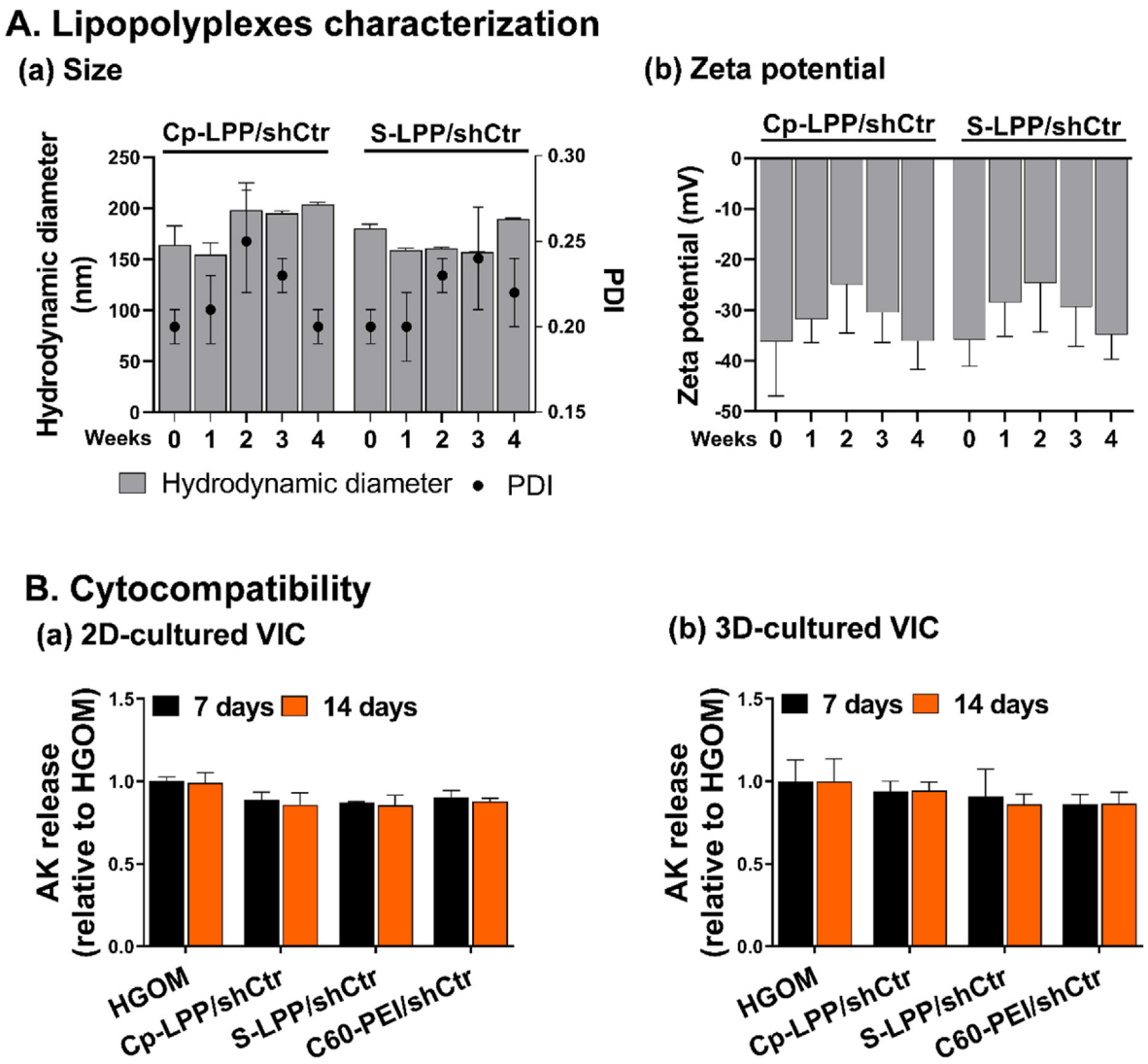

Fig. 1. Characterization of collagen IV-targeted lipopolyplexes encapsulating the shRNA plasmid. Average hydrodynamic diameter and polydispersity indices (**A-a**) and Zeta potential (**A-*b***) of collagen IV-targeted lipopolyplexes (Cp-LPP/shCtr) and non-targeted lipopolyplexes (S-LPP/shCtr); results are reported as mean ± S.D. for three individual measurements. Cytotoxicity assay evaluated as adenylate kinase (AK) release in the culture medium at 48 h after transfection of oVIC seeded on 2D support (**B-a**) and in 3D aortic root-derived hydrogel (**B-b**) performed on the 5th and 12th day; data are presented as mean ± S.D. of four experiments done in duplicates.

calculated for VIC maintained in the NM medium. These results indicate that the synergic action of high glucose concentration and osteogenic factors contribute to VIC osteodifferentiation and collagen IV overexpression.

3.4. Collagen IV-targeted lipopolyplexes are efficiently taken up by HGOM-exposed VIC

The uptake of collagen IV-targeted lipopolyplexes by 2D- or 3D-cultured VIC was evaluated in cells grown (5 days) in NM or HGOM medium. VIC were incubated with lipopolyplexes containing C60-PEI/Cy3-fluorescently labeled plasmid polyplexes and functionalized with a peptide specific for collagen IV (Cp-LPP/Cy3) or a non-specific, scrambled peptide (S-LPP/Cy3) for 48 h, in the absence or presence of an excess concentration of collagen IV binding-peptide (Cp).

2D-cultured VIC. VIC were visualized by fluorescence microscopy after 24 and 48 h of LPP incubation and then processed for flow cytometry. As shown in Fig. 3 A-a and **3 A-b** Cp-LPP/Cy3 are efficiently taken up by VIC, the internalization being increased in the case of HGOM-activated VIC as compared to VIC cultured in NM medium. Measuring the fluorescence intensity signal of the red pixels (ImageJ software version 1.8.0) after 24 h of incubation with Cp-LPP/Cy3, we found a higher number of intracellular red fluorescent dots in the HGOM-activated VIC compared to non-activated VIC; after 48 h their number increased even more (Fig. 3 A-a). In HGOM-activated VIC, regardless of the incubation time (24 or 48 h), the fluorescence intensity of internalized Cp-LPP/Cy3 was always higher than that of S-LPP/Cy3.

In the case of non-activated VIC, there was no significant difference in the fluorescence intensity between the two types of lipopolyplexes. However, after 48 h of incubation, the fluorescence intensity of internalized Cp-LPP/Cy3 was higher than that of S-LPP/Cy3. Furthermore, the Cp-LPP/Cy3 were specifically taken up mainly via collagen IV receptors, as testified by the decreased fluorescence observed when VIC (activated or non-activated) were preincubated with an excess of Cp binding peptide. The results obtained by fluorescence microscopy were validated by flow cytometry experiments (Fig. 3 A-b), which revealed a higher uptake of Cp-LPP/Cy3 by HGOM-activated VIC compared to VIC maintained in the NM medium.

On the other hand, the internalization of S-LPP/Cy3 lipopolyplexes is not dependent on VIC osteodifferentiation, the fluorescence level being

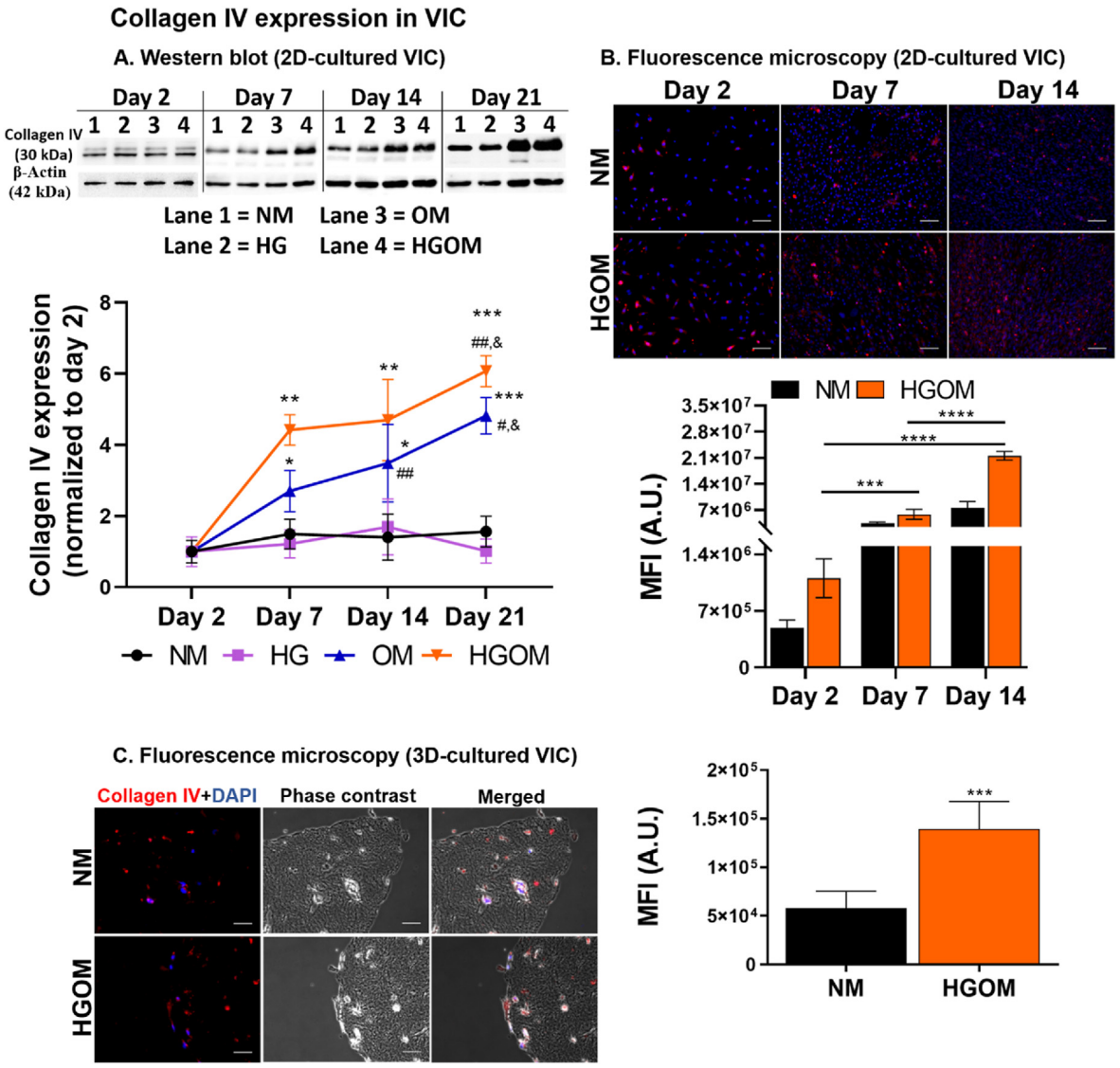

Fig. 2. Collagen IV expression in VIC. (**A**). Representative Western blots depicting collagen IV protein expression in VIC exposed for 2, 7, 14, and 21 days to normal glucose (NM), high glucose (HG) concentrations, medium containing osteogenic factors (OM), and medium containing HG and osteogenic factors (HGOM). Below, is the quantification of the level of collagen IV protein expression as reported to β-actin protein level at different intervals and normalized to the day 2 values. Results represent the means ± S.D. of three independent experiments performed in duplicate (n = 6). *$p < 0.05$, **$p < 0.01$, ***$p < 0.001$ versus values determined on day 2; $^{\#}p < 0.05$, $^{\#\#}p < 0.01$ versus values determined on day 7; $^{\&}p < 0.05$ versus values determined on day 14. (**B**). Representative fluorescence images indicating the presence of collagen IV (red) on 2D support-cultured VIC and grown in NM or HGOM for 2, 7, and 14 days. Nuclei are stained with DAPI (blue). Scale bar: 100 μm. The mean fluorescence of collagen IV was quantified on fluorescence microscopy images (ImageJ software version 1.8.0) and the graph is shown below the images. Results are presented as means ± S.D. of two independent experiments performed in triplicate, three fields per sample. ***$p < 0.001$, ****$p < 0.0001$. (**C, left**). Representative fluorescence and phase contrast images disclosing the presence of collagen IV (red) in VIC seeded in 3D hydrogel and grown in NM or HGOM for 7 days. Nuclei are stained with DAPI (blue). Scale bar: 50 μm. (**C, right**). Quantification of the mean fluorescence of collagen IV on fluorescence microscopy images (ImageJ software version 1.8.0). Results are the means ± S.D. of five fields per sample (n = 3). ***$p < 0.001$ versus values determined on VIC incubated with NM medium.

the same in both non-activated and HGOM-activated VIC. Thereby, the S-LPP/Cy3 lipopolyplexes are internalized through non-specific endocytosis.

In the case of VIC preincubated with an excess of collagen IV-binding peptide, the percentage of internalized Cp-LPP/Cy3 detected on the FL2 channel is ~ 6-times lower compared to the percentage detected in cells without preincubation with excess peptide, suggesting a specific uptake of collagen IV-targeted lipopolyplexes.

3D-cultured VIC. As indicated by the red fluorescence, the HGOM-activated VIC internalized a higher number of nanoparticles after 48 h compared to non-activated VIC (Fig. 3 B). By calculating the mean fluorescence intensity of the Cy3-labeled plasmid, we found a significantly increased uptake of Cp-LPP/Cy3 (~1.25-fold) by HGOM-activated VIC compared to non-activated VIC. Moreover, internalization of Cp-LPP/Cy3 by non-activated and HGOM-activated VIC was higher than S-LPP/Cy3, pointing out that collagen IV-targeted lipopolyplexes are specifically internalized by VIC.

3.5. *Transfection efficiency of collagen IV-targeted lipopolyplexes*

2D-cultured VIC. Five days after exposure of cultured VIC to NM or HGOM medium, the cells were transfected (48 h) with Cp-LPP/pEYFP and S-LPP/pEYFP lipopolyplexes and investigated by fluorescence microscopy (Fig. 4 A-a) and flow cytometry (Fig. 4 A-b). The data showed that in HGOM-activated VIC, the transfection with Cp-LPP/pEYFP had a significantly greater efficiency (two-fold higher) of fluorescent protein

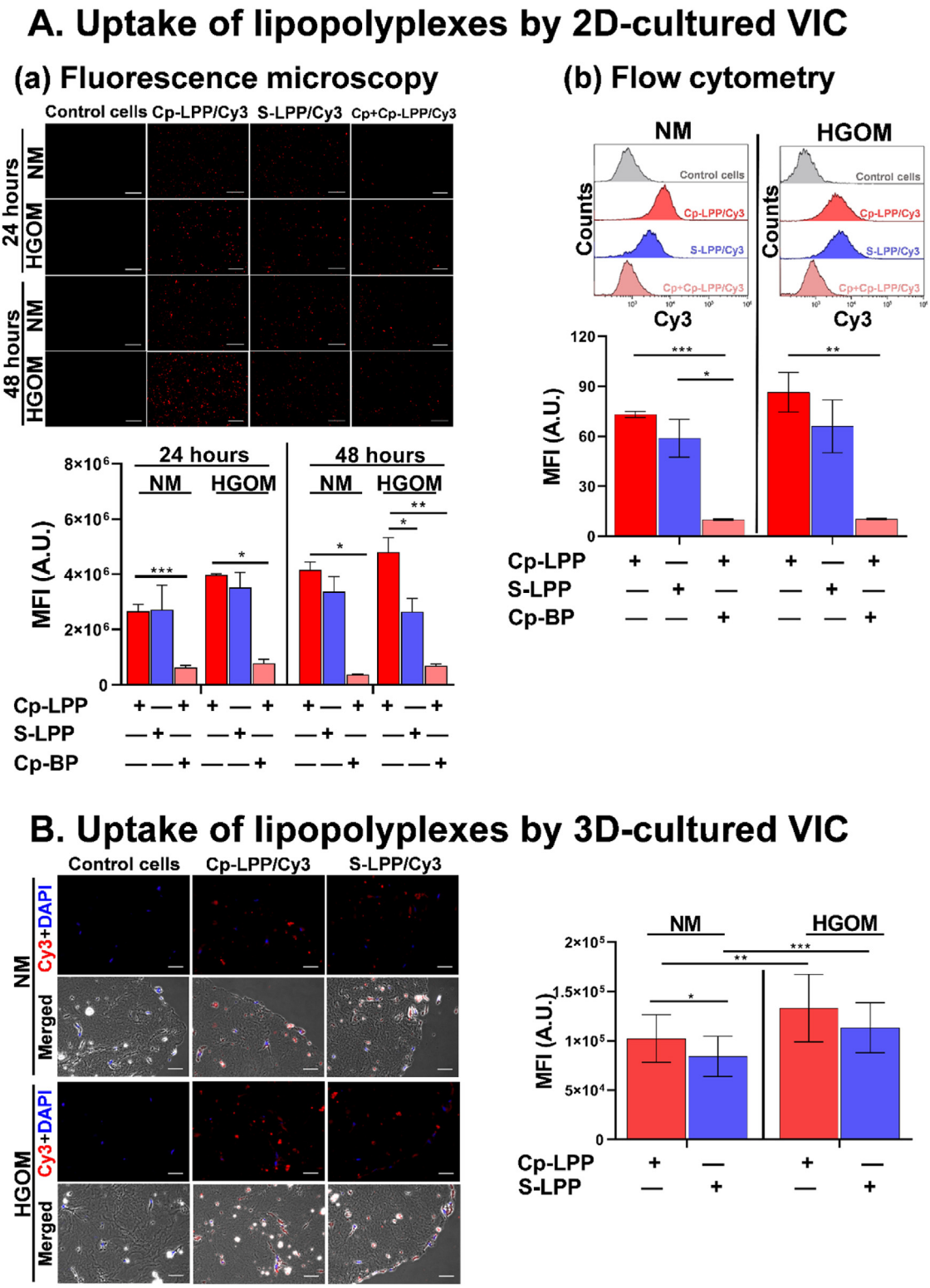

Fig. 3. Uptake of collagen IV-targeted lipopolyplexes by VIC cultured in a 2D (A) or 3D (B)-system. (A-a) Representative fluorescence micrographs of the uptake of fluorescently labeled Cp-LPP/Cy3 and S-LPP/Cy3 (red) by 2D-cultured VIC exposed to NM or HGOM medium for 5 days prior to incubation with lipopolyplexes, in the absence or the presence of an excess of collagen IV-binding peptide (Cp-BP). Scale bar: 200 μm. Quantification of the mean fluorescence is shown below the images. Results are the means ± S.D. of three independent experiments performed in duplicate, five fields per sample. *p < 0.05, **p < 0.01, ***p < 0.001. (A-b) Flow cytometry data showing the uptake of Cp-LPP/Cy3 and S-LPP/Cy3 by 2D-cultured VIC exposed to NM or HGOM for 5 days before incubation with lipopolyplexes in the absence or the presence of excess Cp-BP. The results are the means ± S.D. of three experiments performed in duplicates (n = 6). Representative flow cytometry charts are shown above the graph. (B) Fluorescence and merged (fluorescence and phase contrast) images of Cp-LPP/Cy3 and S-LPP/Cy3 showing the uptake by 3D-cultured VIC exposed to NM or HGOM medium for 5 days prior to before incubation with lipopolyplexes. Scale bar: 50 μm. The quantification of the mean fluorescence is shown on the right. Results are the means ± S.D. of five fields per sample (n = 3). *p < 0.05, **p < 0.01, ***p < 0.001.

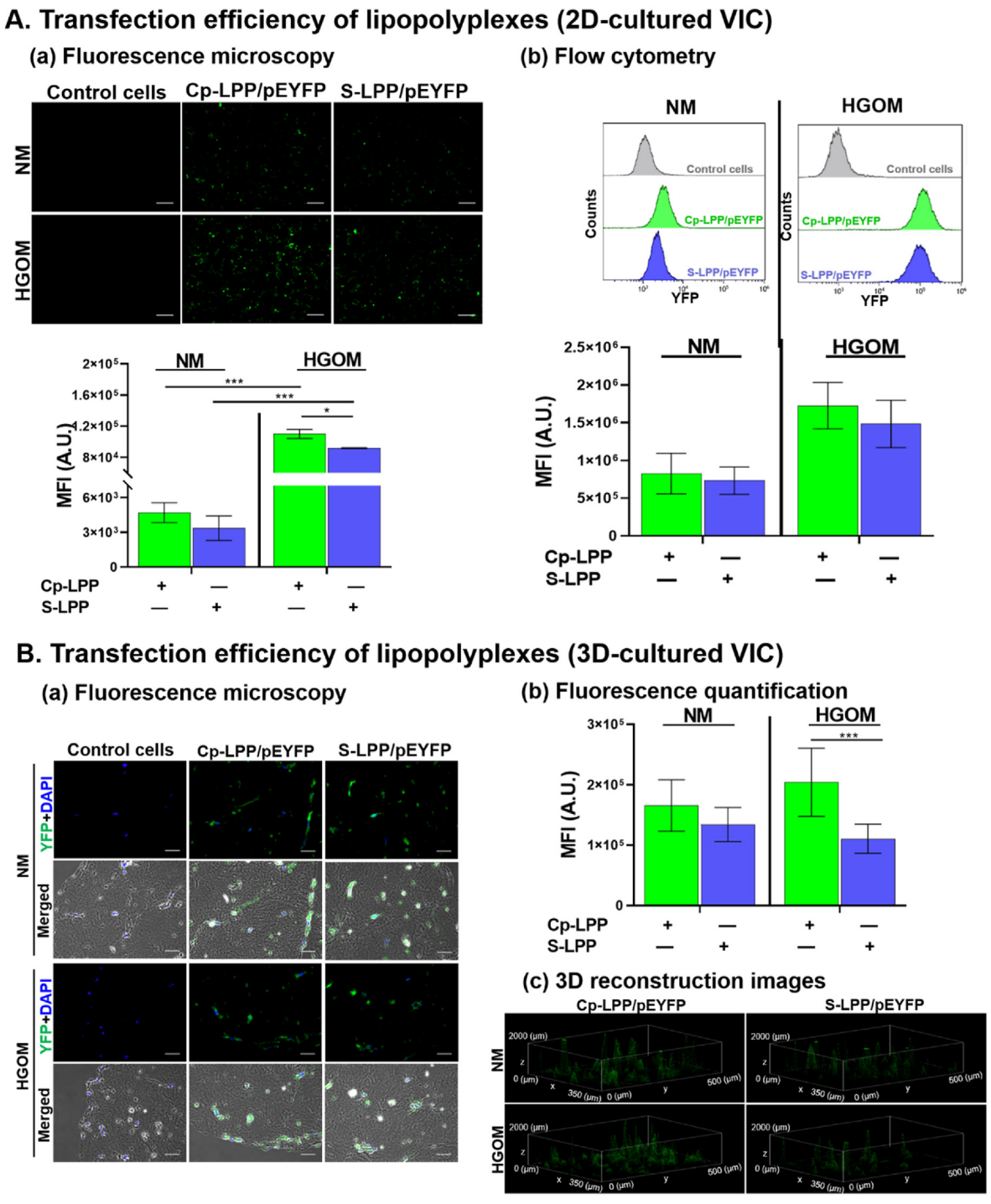

Fig. 4. Transfection efficiency of collagen IV-targeted lipopolyplexes in 2D (A) or 3D (B)-cultured VIC. (A-a) Imaging of the fluorescent protein in 2D-cultured VIC exposed to NM or HGOM medium (for 5 days) before incubation (48 h) with Cp-LPP/pEYFP and S-LPP/pEYFP lipopolyplexes. Scale bar: 100 μm. Below the images, the quantification of the mean fluorescence intensity of the green pixels. The results are shown as means ± S.D. from two experiments performed in duplicates, five random fields per sample. (A-b) Representative flow cytometry charts and data analysis presenting the fluorescent protein expression in 2D-cultured VIC transfected with Cp-LPP/pEYFP and S-LPP/pEYFP lipopolyplexes. The results are shown as means ± S.D. from three experiments performed in duplicates (n = 6). (B-a) Representative images of fluorescence microscopy and phase contrast of Cp-LPP/pEYFP and S-LPP/pEYFP transfection in 3D-cultured VIC and exposed to NM or HGOM medium for (5 days) before incubation with lipopolyplexes. Scale bar: 50 μm. (B-b) Quantification of the mean fluorescence intensity of the green fluorescence, indicative of the expression of the fluorescent protein. Results are the means ± S.D. of five fields per sample (n = 3). (B-c). 3D reconstruction images of Z-stacking sections for 3D-cultured VIC, transfected with Cp-LPP/pEYFP and S-LPP/pEYFP showing the fluorescent protein expression (green) in the cells spread in the hydrogel. Statistics: *$p < 0.05$, ***$p < 0.001$.

expression than in VIC cultured in NM, as resulted from the mean fluorescence intensity measurements of green pixels fluorescence (ImageJ software version 1.8.0) and flow cytometry analysis (Fig. 4 A-a and **4 A-b**, respectively). An increased transfection was also observed for S-LPP/pEYFP in HGOM-activated VIC compared to that in non-activated cells. Although, when comparing the two types of lipopolyplexes, there was no statistically significant difference in the transfection efficiency, the fluorescence measured in VIC transfected with Cp-LPP/pEYFP being slightly higher than that measured in VIC exposed to S-LPP/pEYFP (Fig. 4A a, b).

3D-cultured VIC. A significantly higher expression of the fluorescent protein encoded by pEYFP plasmid (~1.8-fold, <0.001) in HGOM-activated 3D-cultured VIC was found for collagen IV-targeted lipopolyplexes, Cp-LPP/pEYFP when compared with non-targeted (S-LPP/pEYFP) lipopolyplexes (Fig. 4 B-a, b). The fluorescent protein expression in VIC grown in control medium (NM) was slightly higher in cells transfected with Cp-LPP/pEYFP than that transfected with S-LPP/pEYFP, yet with no statistical significance (Fig. 4 B-b). The 3D reconstruction images of 3D-cultured VIC (Fig. 4 B-c) showed the expression of the fluorescent protein in the cells that spread in the depth of the hydrogel. A higher level of green fluorescence may be noticed in the case of transfection with Cp-LPP/pEYFP, indicating a superior transfection efficiency compared to S-LPP/pEYFP.

3.6. In valvular interstitial cells Cp-LPP/shRunx2 lipopolyplexes diminish the expression of osteoblast-specific differentiation markers

The therapeutic effect of Cp-LPP/shRunx2 lipopolyplexes was evaluated by determining the mRNA level of osteogenic molecules in osteodifferentiated VIC cultured in 2D or 3D cell models and transfected with different shRunx2 nanocarriers (Fig. 5)**.** Cultured either in 2D or 3D conditions, the exposure of VIC to HGOM medium for 7 or 14 days determined a significant increase in mRNA gene of Runx2 and other osteogenic proteins (i.e., osteopontin, bone sialoprotein, bone morphogenic protein 2) as compared to control cells. The mRNA level of Runx2 decreased by ~50% in both 2D and 3D-cultured VIC, 48 h after a single transfection with Cp-LPP/shRunx2 (Fig. 5 A). A second transfection of VIC on the 12th day reduced the Runx2 gene expression on the 14th day by 70% ($p < 0.0001$) in 2D-cultured VIC, whereas in 3D-cultured VIC, mRNA-Runx2 remained at the same level as after one transfection (Fig. 5 A-a, A-b). In transfections with S-LPP/shRunx2 lipopolyplexes and C60-PEI/shRunx2 polyplexes, the mRNA-Runx2 expression was also decreased significantly and maintained at the same level for both culture conditions. The Runx2 gene expression was reduced by ~30% compared to the expression by HGOM-activated control cells when transfection was done with Cp-LPP/shRunx2, while transfection with C60-PEI/shRunx2 determined a decrease by ~40%. The lipopolyplexes carrying the control shCtr plasmid, either targeted or non-targeted, did not affect the mRNA-Runx2 expression irrespective of the culture condition, 2D or 3D. At 48 h after the first transfection of cells exposed to HGOM with Cp-LPP/shRunx2, the mRNA-OSP level decreased by ~40% ($p < 0.0001$) in 2D-cultured VIC (Fig. 5 B-a), while in the 3D-cultured cells, the OSP gene expression was reduced even more by ~65% ($p < 0.0001$) as compared with non-transfected cells (Fig. 5 B-b). The OSP level decreased further after the second transfection with Cp-LPP/shRunx2 in 2D-cultured VIC, being ~60% lower than in non-transfected cells, while in 3D-cultured cells, the OSP gene expression was maintained at a level similar to that detected after a single transfection. The transfection on day 5 with S-LPP/shRunx2 also decreased the level of mRNA-OSP measured on day 7 of culture in HGOM by ~40% and ~50% in 2D-, and 3D-cultured VIC, respectively. mRNA-OSP expression was similar (~30% in 2D and ~40% in 3D-cultured VIC) on day 14th after the second transfection performed on the day 12th.

A similar reduction in mRNA-OSP level was determined in the case of oVIC transfected with C60-PEI/shRunx2 polyplexes in both cell culture systems. The transfection of cells with the shRNA (control plasmid) did not significantly affect the OSP mRNA level, regardless of the type of nanoparticle formulations (Fig. 5 B-a, B-b). The mRNA-BSP decreased in VIC cultivated in 2D or 3D conditions after the incubation with nanoparticles carrying shRNA-Runx2 plasmid sequences. The first transfection of 2D-cultured VIC with Cp-LPP/shRunx2 decreased the mRNA-BSP level by ~50% ($p < 0.0001$), while a reduction of ~40% ($p < 0.01$) was achieved when cells were transfected twice, in the 5th and 12th day in comparison with non-transfected HGOM-exposed VIC (Fig. 5 C-a). For VIC grown in the 3D hydrogel after one transfection performed on day 5, the BSP gene expression was reduced by ~40%, decreasing further to ~65% after the second transfection (Fig. 5 C-b). The mRNA-BSP level reduction was also achieved by transfecting 2D and 3D cultured-oVIC with S-LPP/shRunx2, but only by ~25–30% compared to non-transfected cells, regardless of the number of transfection performed. Although in 2D culture, C60-PEI/shRunx2 polyplexes reduced BSP gene expression by ~50% in oVIC, both after a single or a double transfection. In the 3D cell culture, C60-PEI/shRunx2 reduced the mRNA-BSP expression by ~20–30% as compared to non-transfected oVIC. No modification in the mRNA-BSP gene expression was detected in cultured oVIC treated with the control shCtr plasmid formulated in lipopolyplexes (Fig. 5 C-a, C-b).

Interestingly, a significant reduction in BMP2 gene expression was determined in 2D-cultured oVIC after a single transfection with all types of nanoparticles: Cp-LPP/shRunx2 (~50%, $p < 0.0001$), S-LPP/shRunx2 (~50%, $p < 0.0001$) and C60-PEI/shRunx2 (~40%, $p < 0.0001$) (Fig. 5 D-a). After the second transfection on the 12th day with Cp-LPP/shRunx2, S-LPP/shRunx2, and C60-PEI/shRunx2, the mRNA-BMP2 was reduced by ~50% ($p < 0.01$), ~35% ($p < 0.01$) and ~65% ($p < 0.0001$), respectively (Fig. 5 D-a). The results were similar upon transfection of 3D-cultured oVIC (on the 5th day) with all three types of nanoparticles (Fig. 5 D-b) and no significant changes in the down-regulation of BMP2 gene expression was detected after the second transfection. In controls, the cell transfections with lipopolyplexes containing the control shCtr plasmid did not change the mRNA level for BMP2 as compared with non-transfected oVIC (Fig. 5 D-a, D-b).

3.7. Cp-LPP/shRunx2 lipopolyplexes reduce alkaline phosphatase activity and calcium deposits in osteoblast-committed 3D-cultured VIC

We evaluated the alkaline phosphatase (ALP) activity in 3D-grown VIC grown after transfection with shRunx2 plasmid formulated into nanoparticles. The results showed that the enzymatic activity of ALP increased in VIC exposed to HGOM for a period of 14 days by ~60% compared to cells cultivated in the control medium, NM (Fig. 6 A). Cp-LPP/shRunx2 decreased the ALP activity 48 h after a single transfection performed on day 5 by 85% ($p < 0.0001$), while a reduction of ALP activity by ~50% was obtained after transfection of VIC with non-targeted S-LPP/shRunx2 and C60-PEI/shRunx2 polyplexes. After two transfections with shRNA-Runx2 plasmids delivered by lipopolyplexes or polyplexes, the ALP activity decreased by 55% ($p < 0.0001$). No statistically significant inhibition was obtained when shCtr plasmid was used for transfection, either after 7 days or 14 days.

The calcium deposits in 3D-cultured VIC exposed to HGOM were evaluated by a colorimetric method, that determines the calcium concentration in the cell lysates, and by staining the calcium deposits with Alizarin Red. The exposure of the hydrogel containing VIC to HGOM for 7 days determined an increase in the calcium concentration by ~25%, that further increased by ~50% after 14 days of continuous incubation (Fig. 6 B). All three types of nanoparticles, carriers of shRNA-Runx2 plasmids, were effective in blocking the formation of calcium deposits in VIC exposed to the osteogenic medium. A reduction of calcium concentration by 55% ($p < 0.0001$) was obtained when Cp-LPP/shRunx2 was used for VIC transfection. S-LPP/shRunx2 and C60-PEI/shRunx2 polyplexes determined a decrease in the calcium concentration by ~35% and, respectively, ~40%, 48 h after the transfection performed on day 5. The calcium concentration in 3D cultured VIC transfected twice (on days 5

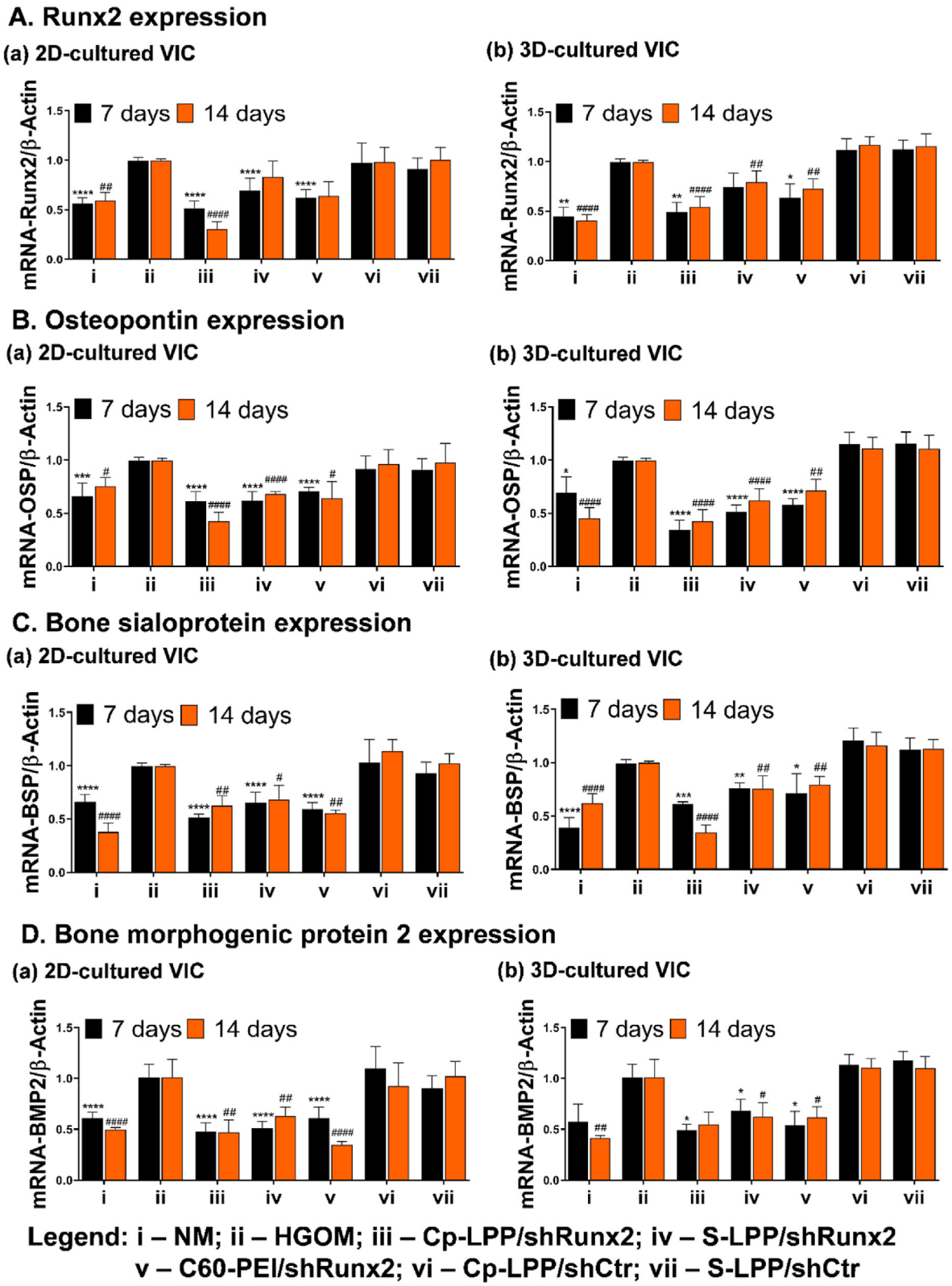

Fig. 5. *Gene expression of osteogenic molecules (**A-D**) in VIC seeded in 2D (**a**)* or 3D *(**b**)* cell *culture models: Runx2 (**A**), osteopontin (**B**), bone sialoprotein (**C**), and bone morphogenic protein 2 (**D**). VIC were transfected on the fifth day and twelfth day of exposure to HGOM with different shRunx2 nanocarriers (Cp-LPP/shRunx2 and S-LPP/shRunx2 lipopolyplexes, and C60-PEI/shRunx2 polyplexes). As controls, Cp-LPP/shCtr, and S-LPP/shCtr were used. The results normalized to β-actin are represented as fold change relative to HGOM (considered as 1) and expressed as mean ± S.D. of three independent experiments made in duplicate (n = 6). *p < 0.05, **p < 0.01, ***p < 0.001, ****p < 0.0001 when compared with HGOM at 7 days; #p < 0.05, ##p < 0.01, ###p < 0.001, ####p < 0.0001 when compared with HGOM at 14 days.*

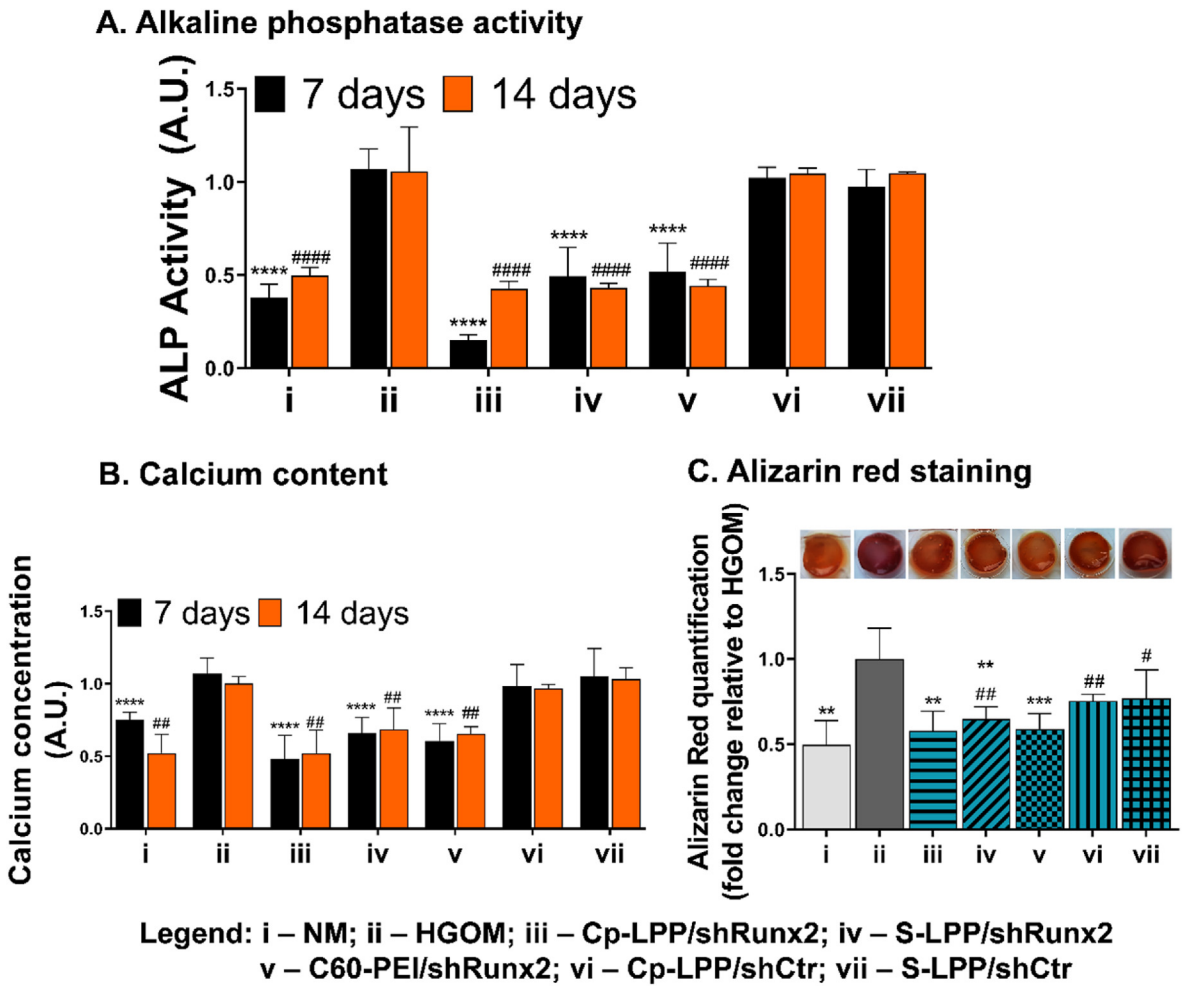

Fig. 6. Cp-LPP/shRunx2 lipopolyplexes reduce the ALP activity and block the formation of calcium deposits. (**A**) Quantitative assay of ALP activity performed at 7 and 14 days after a single transfection of HGOM-activated VIC on day 5 or two transfections (on days 5 and 12) with different nanoparticle formulations. (**B**) Quantitative assay of calcium concentration at 7 and 14 days after a single transfection of HGOM-activated VIC on day 5 or two transfections (on days 5 and 12) with different nanoparticle formulations. For both assays, data are means ± S.D. of three experiments in triplicate and presented as fold change relative to HGOM condition (considered 1). *$p < 0.05$, **$p < 0.01$, ***$p < 0.001$, ****$p < 0.0001$ when compared with HGOM at 7 days; $^{\#}p < 0.05$, $^{\#\#}p < 0.01$, $^{\#\#\#}p < 0.001$, $^{\#\#\#\#}p < 0.0001$ when compared with HGOM at 14 days. (**C**) Alizarin Red-stained calcium deposits in 3D-cultured VIC after 14 days of HGOM exposure and two transfections performed on days 5 and 12 with different nanoparticles. The graph displays the quantitative measurement of the dye released from the hydrogel. Data are means ± S.D. of two experiments made in triplicates and were represented as fold change relative to HGOM condition (considered 1). **$p < 0.01$, ***$p < 0.001$ when compared with HGOM; $^{\#}p < 0.05$, $^{\#\#}p < 0.01$ when compared with NM.

and 12) with shRNA-Runx2 carrying nanoparticles was significantly lower compared to that in VIC cultured in HGOM for 14 days ($p < 0.01$). The calcium concentration decreased by ~50%, ~30%, and ~35% after the second transfection of VIC with Cp-LPP/shRunx2, S-LPP/shRunx2, and C60-PEI/shRunx2, respectively. The VIC exposure to LPP containing shCtr plasmid did not influence the calcium concentration compared to non-transfected VIC.

The results correlate well with calcium staining with Alizarin Red performed on the 14th day, after two transfections of osteoblast-committed 3D cultured VIC with shRNA-Runx2 plasmids formulated into collagen IV-targeted or non-targeted lipopolyplexes (Fig. 6 C). The exposure to the osteogenic medium stimulated the formation of calcific deposits, as observed in the image of hydrogel containing VIC exposed to HGOM. Contrary, the HGOM-exposed cells grown in the 3D model transfected twice with nanoparticles containing shRNA-Runx2 plasmids exhibited lower staining with Alizarin Red. After the quantitative measurement of Alizarin Red released from the hydrogel, we observed that oVIC treatment with Cp-LPP/shRunx2 and C60-PEI/shRunx2 reduced the calcium deposition by ~40%, while the reduction induced by S-LPP/shRunx2 was by ~35% compared to levels determined in HGOM-exposed VIC.

3.8. Collagen IV-targeted lipopolyplexes accumulate at a significantly higher level in the aortic valve of atherosclerotic mice than the non-targeted particles

Collagen IV is overexpressed in the aortic valve of diabetic/hyperlipidemic ApoE-deficient mice. Fluorescence microscopy on cryosections was employed to substantiate the presence of collagen IV in the aortic valve isolated from diabetic/hyperlipidemic ApoE-deficient mice and in C57BL/6 mice, as controls. As expected, in both experimental conditions, positive staining areas of collagen IV were found; however, the staining areas were much more extensive in valve sections of diabetic/hyperlipidemic ApoE-deficient mice (Fig. 7 A).

Collagen IV-targeted lipopolyplexes localization. Next, we investigated whether the biodistribution of Collagen IV-targeted lipopolyplexes is distinct from that of non-targeted ones. The Rhodamine B-labeled Cp-LPP/shCtr or S-LPP/shCtr lipoplexes (1.5 mg of plasmid/kg body weight)

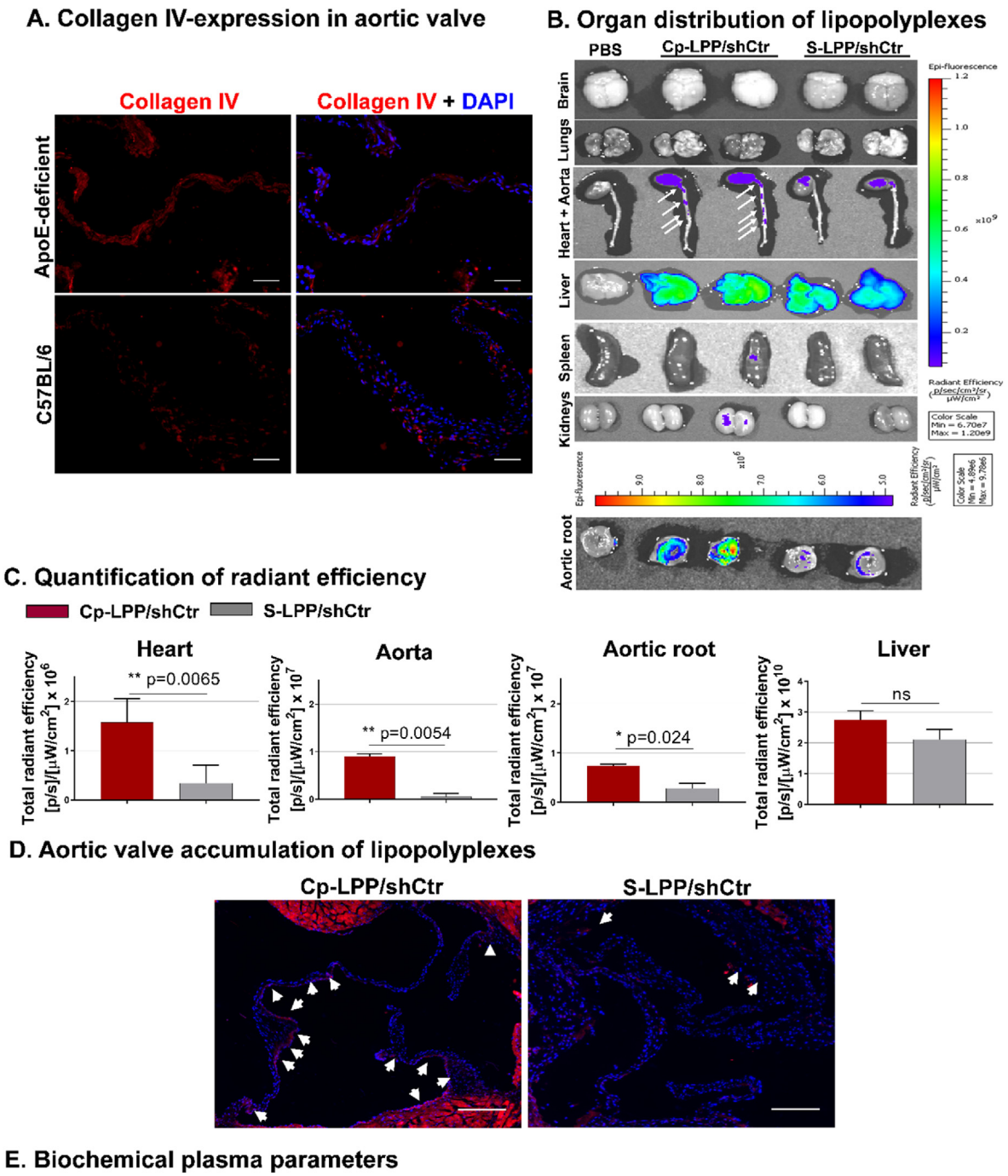

E. Biochemical plasma parameters

Experimental group	Liver function parameters			Kidney function parameters	
	ALT (U/L)	AST (U/L)	ALP (U/L)	BUN (mg/dL)	Creatinine (mg/dL)
PBS	6.5 ± 0.2	23 ± 11.5	10.9 ± 1	25.5 ± 4	0.3 ± 0.1
Cp-LPP/shCtr	8.2 ± 1.2	25.1 ± 4.5	6.9 ± 1.2	30.1 ± 4.2	0.34 ± 0.08
S-LPP/shCtr	9.2 ± 3	20.1 ± 0.8	10.3 ± 3	25.1 ± 1	0.1 ± 0.05

Fig. 7. (**A**) Collagen IV expression in the aortic valve. Representative fluorescence images of aortic root cryosections from diabetic/hyperlipidemic ApoE-deficient mice and C57BL/6 mice stained for collagen IV (red) and counterstained with DAPI (blue) to identify the nuclei; Scalebar: 200 μm. (**B**) Localization of fluorescently labeled lipopolyplexes either targeted to collagen IV (Cp-LPP/shCtr) or non-targeted (S-LPP/shCtr) in organs harvested from diabetic/hyperlipidemic ApoE-deficient mice injected with lipopolyplexes. Measurements were recorded 90 min after retroorbital administration employing an IVIS Spectrum imaging system Caliper 200, by detection of Rhodamine B fluorescence λex = 535 nm and λem = 620 nm. (**C**) Quantification of total radiant efficiency in heart, aorta, liver, and aortic root. (**D**) Representative images of Rhodamine B-labeled Cp-LPP/shCtr and S-LPP/shCtr lipopolyplexes (red) distribution in the aortic valve sections of diabetic/hyperlipidemic ApoE-deficient mice. Nuclei labeled with DAPI (blue); white arrows depict the accumulation of lipopolyplexes. Scale bar: 300 μm. (**E**) Biochemical parameters for liver (ALT, AST, ALP) and kidney function (BUN and creatinine) measured in the plasma of C57BL/6 control mice (injected with PBS) or mice treated with lipopolyplexes targeted to collagen IV (Cp-LPP/shCtr) or non-targeted (S-LPP/shCtr). Data are mean ± S.D. (n = 3 mice for each group).

were administered by retro-orbital injection to diabetic/hyperlipidemic ApoE-deficient mice. After 90 min, the vasculature was washed free of blood and the brain, lungs, liver, spleen, kidneys, heart with aortas, and aortic roots were harvested and investigated *ex vivo* using the IVIS Caliper 200 imaging system. The ROI (region-of-interest) function of Living Image 4.3.1. software was used to quantify the radiant efficiency [fluorescence emission radiance per incident excitation intensity (p/s/cm^2/sr)/(μW/cm^2)] of isolated tissues. The autofluorescence of organs isolated from mice injected with PBS was subtracted from the ROI values measured for each organ.

The results showed that both Cp-LPP/shCtr and S-LPP/shCtr lipopolyplexes accumulate mainly in the liver, the heart, and the aortas (Fig. 7 B). The other organs have a reduced level of fluorescence measured at a wavelength specific to Rhodamine B. There was a statistically significant increased accumulation of Cp-LPP/shCtr in the heart, aortic root, and aorta of mice, compared with S-LPP/shCtr. According to the measured radiant efficiency presented in Fig. 7 C, the collagen IV-targeted lipopolyplexes accumulated at a higher level in the heart and aorta of ApoE-deficient mice than non-targeted lipopolyplexes (S-LPP/shCtr) by 18-fold and 4.7-fold, respectively. Although the accumulation of Cp-LPP/shCtr in the liver was higher than that of S-LPP/shCtr, the difference was not statistically significant.

To further validate the above results, the aortic sinuses were isolated from diabetic/hyperlipidemic ApoE-deficient mice injected with Rhodamine B-labeled Cp-LPP/shCtr and S-LPP/shCtr, and cryosections were examined by fluorescence microscope. The red fluorescence signal, indicative of the localization of lipopolyplexes, was found in aortic valve leaflets with a higher accumulation detected for collagen IV-targeted lipopolyplexes as compared with S-LPP/shCtr (Fig. 7 D).

3.9. Lipopolyplexes are safe for in vivo administration

Twenty-four hours after retro-orbital injection of Cp-LPP/shCtr and S-LPP/shCtr lipopolyplexes in wild-type C57BL/6 mice, a set of plasma biochemical parameters were determined (Fig. 7 E). No change in the liver (AST, ALT, ALP) and renal (urea, creatinine) functional parameters were noticed compared to those measured in control mice injected with PBS.

4. Discussion

In the development of calcific aortic valve disease (CAVD), the valve stenosis and calcification processes are driven by VIC, cells that switch to an osteogenic phenotype in response to pathological stimuli, such as high blood pressure, inflammatory cytokines, and growth factors [29]. The quest for an available pharmacological treatment for CAVD is intense. It was reported the key role of transcriptional factor Runx2 in the transition of VIC from a fibroblast-like, to an osteoblast-like phenotype [30–32]. Therefore, a strategy intended to silence Runx2 may be a suitable therapeutic option for CAVD. Others and we showed that the downregulation of Runx2 in osteoblast-committed VIC by siRNA/shRNA or miRNA alleviates cells' osteodifferentiation by reducing the expression of osteogenic genes and blocking calcium deposition [18,19,33,34]. In this study, we took a step forward and designed lipopolyplexes targeted to collagen IV and carrying shRNA-Runx2 (Cp-LPP/shRunx2) and investigated whether they affect the osteogenic differentiation of VIC. We employed a 3D culture model (similar to a native extracellular matrix) cultivated with VIC exposed to an osteogenic medium to induce the osteogenic differentiation of cells. Previously, a 3D-printed model of CAVD containing human VIC exposed to an osteogenic medium was used to investigate the endocytosis of Cy5.5-labeled gold nanoparticles (AuNPs) functionalized with miRNA by VIC [35].To validate the results *in vivo*, we used the diabetic/hyperlipidemic ApoE-deficient mouse and studied the effect of Cp-LPP/shRunx2 on functional parameters of the liver and kidney, and the ability to localize and accumulate in the pathological valve leaflets.

Our comparative experiments support the concept that the *in vitro* use of 3D scaffolds to grow cells offers results that are closer to the *in vivo* conditions. The 3D systems allow the embedded cells to interact with each other and with the ECM in a 3D environment, mimicking the tissue they come from Refs. [36,37]. Previously, we developed a 3D hydrogel obtained from the porcine cell-free native aortic root and showed that, unlike 2D rigid substrates, VIC cultured in this hydrogel maintained the fibroblast-like phenotype [24]. Furthermore, the exposure of 3D-cultured VIC to osteogenic conditions determined the overexpression of Runx2 and the formation of calcium deposits, making this model suitable for VIC osteodifferentiation studies [24].

Here, an RNA interference nanosystem directed to the ECM protein, collagen IV, was developed and employed for shRNA-Runx2 delivery to osteoblast-differentiated VIC (oVIC) grown in the 3D hydrogel and to the aortic valve after *in vivo* administration. As we recently described [19], in the present study we prepared lipopolyplexes (LPP) consisting of a negatively charged lipid bilayer covering the complexes of shRNA-Runx2 plasmid and C60-PEI made by the electrostatic assembly. At the surface of LPP, a peptide (Cp) described to bind selectively and with high affinity to collagen IV [21] was coupled. We envisaged collagen IV as an appropriate target assuring a high specificity of shRNA nanocarriers for the dysfunctional aortic valves. Collagen IV is suitable for targeting VIC in diseased aortic valves since we demonstrated its increased expression by VIC exposed to an osteogenic medium and in the aortic valve leaflets of diabetic/hyperlipidemic ApoE-deficient mice. This abundance of collagen IV was found also in the basal lamina of aortic valves isolated from patients with ischemic cardiomyopathy [38]. The high expression and accessibility ensured by the denudation of the valvular endothelium in CAVD [39] make collagen IV an attractive target for the specific accumulation of collagen IV-directed nanoparticles into aortic valve leaflets. Former reports used collagen IV-targeted nanoparticles for drug delivery to the sites of vascular injury [21,40–42]. Moreover, collagen IV was successfully employed for targeting atherosclerotic plaque in mice [43]. It was shown that collagen IV-targeted polymeric nanoparticles containing pro-resolving annexin A1-derived peptide [44] or the anti-inflammatory cytokine interleukin 10 [45] stabilize vulnerable plaques by promoting inflammation resolution.

The collagen IV-targeted (Cp-LPP/shCtr) and scrambled peptide-coupled (S-LPP/shCtr) lipopolyplexes have an average hydrodynamic diameter of about 200 nm and negative Zeta potential, features that make them suitable for *in vivo* administration. It was shown that positively charged nanoparticles are more prone to non-specific interactions with cell membranes than negatively charged ones [46]. The VIC viability, assessed by measuring the adenylate kinase (AK) released from dying cells, is not significantly modified by incubation of 2D- and 3D-cultured VIC with Cp-LPP/shCtr and S-LPP/shCtr, after a single or double transfection, recommending lipopolyplexes as biocompatible materials according to International Organization for Standardization, ISO 10993–5:2009 "Biological Evaluation of Medical Devices Part 5: Tests for in Vitro Cytotoxicity, 2009".

Collagen IV-targeted lipopolyplexes are taken up by cultured oVIC seeded on 2D support and 3D hydrogel in a significantly higher proportion than non-targeted lipopolyplexes. The competition experiments, done in the presence of an excess of collagen IV-binding peptide, demonstrated that collagen IV-targeted lipopolyplexes are specifically internalized by HGOM-induced oVIC. There are reasons to believe that the uptake of collagen IV-targeted lipopolyplexes by VIC may occur via the receptor urokinase plasminogen activator receptor-associated protein (uPARAP)/Endo180 as demonstrated in primary mouse fibroblasts [47], but the exact mechanism involved in the internalization process needs further investigation. Nevertheless, as proof of the efficient internalization of collagen IV-targeted lipopolyplexes and their functional role, stands the expression of the fluorescent protein coded by pEYFP plasmid entrapped into lipopolyplexes used for transfection of 2D- and 3D-cultured oVIC. Altogether, the small size, the negative surface charge, and the low cytotoxicity of the collagen IV-targeted lipopolyplexes, in conjunction with their efficient uptake by cultured VIC and the results

obtained *in vivo*, propose these nanoparticles as appropriate vectors for shRNA-Runx2 delivery to oVIC. A strong proof and possible mechanism for the therapeutic effect of collagen IV-targeted lipopolyplexes is the reduction of osteogenic gene expression of Runx2, OSP, BSP, and BMP2 in HGOM-exposed VIC, cultured in 3D hydrogel at 48 h after transfection with Cp-LPP/shRunx2 (at the days 5 and 12 of VIC exposure to HGOM). In addition, Cp-LPP/shRunx2 treatment decreased ALP activity and calcium deposition in 3D hydrogel-seeded VIC. These data corroborate well with the *in vivo* results, which showed that i.v. injected collagen IV-targeted lipopolyplexes accumulate in the aortic valve of diabetic/hyperlipidemic ApoE-deficient mice, a fact that justifies further testing to preclinically validate the therapeutic effect of this nano-vector for RNAi in a CAVD model. To the best of our knowledge, this is the first study showing that collagen IV-targeted lipopolyplexes accumulate in the aortic valve of a murine model of diabetes complicated with atherosclerosis and that these nanoparticles deliver shRNA sequences specific for Runx2 and alleviate the osteodifferentiation of VIC cultured in a 3D system mimicking *in vivo* conditions. There are few reports on nanoparticle-based approaches to diagnose and treat experimental models of CAVD. A previous report demonstrated a successful targeting of platelet membrane-coated polymeric nanoparticles to the sclerotic aortic valve of ApoE-deficient mice kept on a western-type diet for 36 weeks [48]. Another group developed superparamagnetic iron oxide nanoparticles (SPIONs) targeted to hydroxyapatite as magnetic resonance imaging (MRI) contrast agents for the earlier detection of CAVD [49,50]. Also, an ex-vivo specific binding of $\alpha\nu\beta3$ integrin targeted perfluorocarbon (PFC) nanoparticles to neovasculature of the aortic valve leaflets excised from cholesterol-fed rabbits suggested the potential of these nanoparticles to detect early angiogenesis in sclerotic aortic valves by MRI [51]. Together, our data and those reported by other groups have shown that a targeted nanoparticle-mediated transport of diagnostic or therapeutic agents to the diseased aortic valve is achievable. In follow-up experiments, we envisage investigating the therapeutic effects of Cp-LPP/shRunx2 in the murine model of diabetes-accelerated atherosclerosis with early aortic valve dysfunction before significant fibrosis and calcification occurrence to study the effect of nanoparticles in inhibition of CAVD progression and, also in ApoE-deficient mice kept on HFD for a longer time, when aortic valve calcification occurs to explore whether the nanocarriers can have an impact on the already calcified valves.

5. Conclusions

We successfully synthesized, and physico-chemical characterized collagen IV-targeted lipopolyplexes formed of C60-PEI/shRunx2 polyplexes encapsulated into an anionic lipid bilayer. Collagen IV-targeted lipopolyplexes carrying shRNA specific for Runx2 silencing hold the following features: (i) are cytocompatible; (ii) are efficiently taken up by oVIC; (iii) diminish the osteodifferentiation of human VIC by a mechanism involving, at least in part, the reduction of several osteogenic molecules expression, alkaline phosphatase activity, and calcium concentration; and (iv) are preferentially recruited to the aortic valve leaflets in diabetic/hyperlipidemic mice. Together, these properties recommend the Cp-LPP/shRunx2 as a novel targeted nanotherapy for CAVD, having the potential to be introduced in clinical practice.

6. Compliance with ethics requirements

All Institutional and National Guidelines for the care and use of animals were followed. The experiments were approved by the Ethics Committee of the Institute of Cellular Biology and Pathology "Nicolae Simionescu" and by the National Sanitary Veterinary and Food Safety Authority authorization no. 448/April 02, 2019 and were performed in accordance with the Romanian Law no. 43/2014 (Official Monitor, Part I nr. 326 pages 2–4), which transposes the EU directive 2010/63/EU on the protection of animals used for scientific purposes.

Credit author statement

Geanina Voicu: Methodology, Investigation, Formal analysis, Validation, Visualization, Writing - original draft. **Cristina Ana Mocanu**: Methodology, Investigation, Formal analysis, Validation, Visualization. **Florentina Safciuc**: Methodology, Investigation. **Maria Anghelache**: Methodology, Investigation, Visualization. **Mariana Deleanu**: Methodology, Investigation, Validation. Sergiu Cecoltan: Methodology. **Mariana Pinteala**: Methodology, Writing - review, and editing. **Cristina Mariana Uritu**: Methodology. **Ionel Droc**: Methodology, Writing - review, and editing. **Maya Simionescu**: Supervision, Writing – review, and editing. **Ileana Manduteanu**: Project administration, Funding acquisition, Writing - review, and editing. **Manuela Calin**: Conceptualization, Supervision, Funding acquisition, Writing - original draft, review, and editing.

Declaration of competing interest

The authors declare that they have no known competing financial interests or personal relationships that could have appeared to influence the work reported in this paper.

Data availability

Data will be made available on request.

Acknowledgments

This work was supported by the Competitiveness Operational Programme 2014–2020, Priority Axis1/Action 1.1.4/, Financing Contract no.115/September 13, 2016/MySMIS:104362, by the Romanian Ministry of Research, Innovation, and Digitization, CNCS-UEFISCDI, project number PN–III–P4-ID-PCE-2020-2465 (contract no. PCE 68/2021), within PNCDI III and by the Romanian Academy.

References

[1] P. Mathieu, R. Bouchareb, M.-C. Boulanger, Innate and adaptive immunity in calcific aortic valve disease, J Immunol Res (2015) 1–11, https://doi.org/10.1155/2015/851945, 2015.

[2] N.M. Rajamannan, The role of Lrp5/6 in cardiac valve disease: experimental hypercholesterolemia in the ApoE−/−/Lrp5−/− mice, J. Cell. Biochem. 112 (2011) 2987–2991, https://doi.org/10.1002/jcb.23221.

[3] J. Natorska, E. Wypasek, G. Grudzień, D. Sobczyk, G. Marek, G. Filip, J. Sadowski, A. Undas, Does diabetes accelerate the progression of aortic stenosis through enhanced inflammatory response within aortic valves? Inflammation 35 (2012) 834–840, https://doi.org/10.1007/s10753-011-9384-7.

[4] M. Banovic, L. Athithan, G.P. McCann, Aortic stenosis and diabetes mellitus: an ominous combination, Diabetes Vasc. Dis. Res. 16 (2019) 310–323, https://doi.org/10.1177/1479164118820657.

[5] S.C. Larsson, A. Wallin, N. Håkansson, O. Stackelberg, M. Bäck, A. Wolk, Type 1 and type 2 diabetes mellitus and incidence of seven cardiovascular diseases, Int. J. Cardiol. 262 (2018), https://doi.org/10.1016/j.ijcard.2018.03.099.

[6] J. Ljungberg, B. Johansson, K.G. Engström, E. Albertsson, P. Holmer, M. Norberg, I.A. Bergdahl, S. Söderberg, Traditional cardiovascular risk factors and their relation to future surgery for valvular heart disease or ascending aortic disease: a case-referent study, J. Am. Heart Assoc. 6 (2017), https://doi.org/10.1161/JAHA.116.005133.

[7] T. Mazzone, A. Chait, J. Plutzky, Cardiovascular disease risk in type 2 diabetes mellitus: insights from mechanistic studies, Lancet 371 (2008), https://doi.org/10.1016/S0140-6736(08)60768-0.

[8] R. Katz, M.J. Budoff, J. Takasu, D.M. Shavelle, A. Bertoni, R.S. Blumenthal, P. Ouyang, N.D. Wong, K.D. O'Brien, Relationship of metabolic syndrome with incident aortic valve calcium and aortic valve calcium progression: the multi-ethnic study of atherosclerosis (MESA), Diabetes 58 (2009), https://doi.org/10.2337/db08-1515.

[9] J. Mosch, C.A. Gleissner, S. Body, E. Aikawa, Histopathological assessment of calcification and inflammation of calcific aortic valves from patients with and without diabetes mellitus, Histol. Histopathol. 32 (2017), https://doi.org/10.14670/HH-11-797.

[10] M.P.O. Virtanen, J. Airaksinen, M. Niemelä, T. Laakso, A. Husso, M.P. Jalava, T. Tauriainen, P. Maaranen, E.-M. Kinnunen, S. Dahlbacka, S. Rosato, M. Savontaus, T. Juvonen, M. Laine, T. Mäkikallio, A. Valtola, P. Raivio, M. Eskola, F. Biancari, Comparison of survival of transfemoral transcatheter aortic valve implantation versus surgical aortic valve replacement for aortic stenosis in low-risk patients

without coronary artery disease, Am. J. Cardiol. 125 (2020) 589–596, https://doi.org/10.1016/j.amjcard.2019.11.002.
[11] S.J. Head, M. Çelik, A.P. Kappetein, Mechanical versus bioprosthetic aortic valve replacement, Eur. Heart J. 38 (2017), https://doi.org/10.1093/eurheartj/ehx141.
[12] B. Alushi, L. Curini, M.R. Christopher, H. Grubitzch, U. Landmesser, A. Amedei, A. Lauten, Calcific aortic valve disease-natural history and future therapeutic strategies, Front. Pharmacol. 11 (2020), https://doi.org/10.3389/fphar.2020.00685.
[13] L. Ciortan, R.D. Macarie, S. Cecoltan, M. Vadana, M.M. Tucureanu, A.C. Mihaila, I. Droc, E. Butoi, I. Manduteanu, Chronic high glucose concentration induces inflammatory and remodeling changes in valvular endothelial cells and valvular interstitial cells in a gelatin methacrylate 3D model of the human aortic valve, Polymers 12 (2020) 2786, https://doi.org/10.3390/polym12122786.
[14] E.J. Farrar, V. Pramil, J.M. Richards, C.Z. Mosher, J.T. Butcher, Valve interstitial cell tensional homeostasis directs calcification and extracellular matrix remodeling processes via RhoA signaling, Biomaterials 105 (2016), https://doi.org/10.1016/j.biomaterials.2016.07.034.
[15] E.R. Mohler, F. Gannon, C. Reynolds, R. Zimmerman, M.G. Keane, F.S. Kaplan, Bone Formation and inflammation in cardiac valves, Circulation 103 (2001) 1522–1528, https://doi.org/10.1161/01.CIR.103.11.1522.
[16] E. Nagy, P. Eriksson, M. Yousry, K. Caidahl, E. Ingelsson, G.K. Hansson, A. Franco-Cereceda, M. Bäck, Valvular osteoclasts in calcification and aortic valve stenosis severity, Int. J. Cardiol. 168 (2013) 2264–2271, https://doi.org/10.1016/j.ijcard.2013.01.207.
[17] N.M. Rajamannan, M. Subramaniam, D. Rickard, S.R. Stock, J. Donovan, M. Springett, T. Orszulak, D.A. Fullerton, A.J. Tajik, R.O. Bonow, T. Spelsberg, Human aortic valve calcification is associated with an osteoblast phenotype, Circulation 107 (2003) 2181–2184, https://doi.org/10.1161/01.CIR.0000070591.21548.69.
[18] G. Voicu, D. Rebleanu, C.A. Constantinescu, E.V. Fuior, L. Ciortan, I. Droc, C.M. Uritu, M. Pinteala, I. Manduteanu, M. Simionescu, M. Calin, Nano-polyplexes mediated transfection of runx2-shRNA mitigates the osteodifferentiation of human valvular interstitial cells, Pharmaceutics 12 (2020) 507, https://doi.org/10.3390/pharmaceutics12060507.
[19] M.C. Geanina, Voicu 1, daniela rebleanu 1, cristina ana Mocanu 1, gabriela tanko 2, ionel droc 3, cristina mariana Uritu 4 5, mariana pinteala 4, ileana manduteanu 1, maya Simionescu 1, VCAM-1 targeted lipopolyplexes as vehicles for efficient delivery of shRNA-runx2 to osteoblast-differentiated valvular interstitial cells; implications in calcific valve disease treatment, Int. J. Mol. Sci. 23 (2022) 3824–3847.
[20] C.M. Uritu, C.D. Varganici, L. Ursu, A. Coroaba, A. Nicolescu, A.I. Dascalu, D. Peptanariu, D. Stan, C.A. Constantinescu, V. Simion, M. Calin, S.S. Maier, M. Pinteala, M. Barboiu, Hybrid fullerene conjugates as vectors for DNA cell-delivery, J. Mater. Chem. B 3 (2015) 2433–2446, https://doi.org/10.1039/C4TB02040E.
[21] J.M. Chan, L. Zhang, R. Tong, D. Ghosh, W. Gao, G. Liao, K.P. Yuet, D. Gray, J.W. Rhee, J. Cheng, G. Golomb, P. Libby, R. Langer, O.C. Farokhzad, Spatiotemporal controlled delivery of nanoparticles to injured vasculature, Proc. Natl. Acad. Sci. U. S. A. 107 (2010), https://doi.org/10.1073/pnas.0914585107.
[22] E.V. Fuior, C.A. Mocanu, M. Deleanu, G. Voicu, M. Anghelache, D. Rebleanu, M. Simionescu, M. Calin, Evaluation of VCAM-1 targeted naringenin/indocyanine green-loaded lipid nanoemulsions as theranostic nanoplatforms in inflammation, Pharmaceutics 12 (2020) 1066, https://doi.org/10.3390/pharmaceutics12111066.
[23] World Medical Association, Declaration of Helsinki: recommendations guiding physicians in biomedical Research involving human subjects, JAMA, J. Am. Med. Assoc. 277 (1997), https://doi.org/10.1001/jama.1997.03540350075038.
[24] S. Cecoltan, L. Ciortan, R.D. Macarie, M. Vadana, A.C. Mihaila, M. Tucureanu, M.-L. Vlad, I. Droc, M. Gherghiceanu, A. Simionescu, D.T. Simionescu, E. Butoi, I. Manduteanu, High glucose induced changes in human VEC phenotype in a 3D hydrogel derived from cell-free native aortic root, Front Cardiovasc Med 8 (2021), https://doi.org/10.3389/fcvm.2021.714573.
[25] M. Turtoi, M. Anghelache, S.M. Bucatariu, M. Deleanu, G. Voicu, F. Safciuc, I. Manduteanu, G. Fundueanu, M. Simionescu, M. Calin, A novel platform for drug testing: biomimetic three-dimensional hyaluronic acid-based scaffold seeded with human hepatocarcinoma cells, Int. J. Biol. Macromol. 185 (2021), https://doi.org/10.1016/j.ijbiomac.2021.06.174.
[26] M. Vadana, S. Cecoltan, L. Ciortan, R.D. Macarie, M.M. Tucureanu, A.C. Mihaila, I. Droc, E. Butoi, I. Manduteanu, Molecular mechanisms involved in high glucose-induced valve calcification in a 3D valve model with human valvular cells, J. Cell Mol. Med. 24 (2020) 6350–6361, https://doi.org/10.1111/jcmm.15277.
[27] M.M. Tucureanu, A. Filippi, N. Alexandru, C. Ana Constantinescu, L. Ciortan, R. Macarie, M. Vadana, G. Voicu, S. Frunza, D. Nistor, A. Simionescu, D.T. Simionescu, A. Georgescu, I. Manduteanu, Diabetes-induced early molecular and functional changes in aortic heart valves in a murine model of atherosclerosis, Diabetes Vasc. Dis. Res. 16 (2019) 562–576, https://doi.org/10.1177/1479164119874469.
[28] K.L. Sider, M.C. Blaser, C.A. Simmons, Animal models of calcific aortic valve disease, Int. J. Inflamm. (2011) 1–18, https://doi.org/10.4061/2011/364310, 2011.
[29] D.A. Towler, Molecular and cellular aspects of calcific aortic valve disease, Circ. Res. 113 (2013), https://doi.org/10.1161/CIRCRESAHA.113.300155.
[30] S. Dharmarajan, M.Y. Speer, K. Pierce, J. Lally, E.M. Leaf, M.-E. Lin, M. Scatena, C.M. Giachelli, Role of Runx2 in calcific aortic valve disease in mouse models, Front Cardiovasc Med 8 (2021), https://doi.org/10.3389/fcvm.2021.687210.
[31] E.E. Wirrig, R.B. Hinton, K.E. Yutzey, Differential expression of cartilage and bone-related proteins in pediatric and adult diseased aortic valves, J. Mol. Cell. Cardiol. 50 (2011) 561–569, https://doi.org/10.1016/j.yjmcc.2010.12.005.
[32] S. Guauque-Olarte, D. Messika-Zeitoun, A. Droit, M. Lamontagne, J. Tremblay-Marchand, E. Lavoie-Charland, N. Gaudreault, B.J. Arsenault, M.-P. Dubé, J.-C. Tardif, S.C. Body, J.G. Seidman, C. Boileau, P. Mathieu, P. Pibarot, Y. Bossé, Calcium signaling pathway genes *RUNX2* and *CACNA1C* are associated with calcific aortic valve disease, Circ Cardiovasc Genet 8 (2015) 812–822, https://doi.org/10.1161/CIRCGENETICS.115.001145.
[33] Y. Wang, S. Chen, C. Deng, F. Li, Y. Wang, X. Hu, F. Shi, N. Dong, MicroRNA-204 targets Runx2 to attenuate BMP-2-induced osteoblast differentiation of human aortic valve interstitial cells, J. Cardiovasc. Pharmacol. 66 (2015), https://doi.org/10.1097/FJC.0000000000000244.
[34] T. Toshima, T. Watanabe, T. Narumi, Y. Otaki, T. Shishido, T. Aono, J. Goto, K. Watanabe, T. Sugai, T. Takahashi, M. Yokoyama, D. Kinoshita, H. Tamura, S. Kato, S. Nishiyama, T. Arimoto, H. Takahashi, T. Miyamoto, M. Sadahiro, M. Watanabe, Therapeutic inhibition of microRNA-34a ameliorates aortic valve calcification via modulation of Notch1-Runx2 signalling, Cardiovasc. Res. 116 (2019), https://doi.org/10.1093/cvr/cvz210.
[35] C.F.T. Van Der Ven, M.W. Tibbitt, J. Conde, A. Van Mil, J. Hjortnaes, P.A. Doevendans, J.P.G. Sluijter, E. Aikawa, R.S. Langer, Controlled delivery of gold nanoparticle-coupled miRNA therapeutics: via an injectable self-healing hydrogel, Nanoscale 13 (2021), https://doi.org/10.1039/d1nr04973a.
[36] F. Pampaloni, E.G. Reynaud, E.H.K. Stelzer, The third dimension bridges the gap between cell culture and live tissue, Nat. Rev. Mol. Cell Biol. 8 (2007) 839–845, https://doi.org/10.1038/nrm2236.
[37] M. Ravi, V. Paramesh, S.R. Kaviya, E. Anuradha, F.D.P. Solomon, 3D cell culture systems: advantages and applications, J. Cell. Physiol. 230 (2015) 16–26, https://doi.org/10.1002/jcp.24683.
[38] A. Weymann, B. Schmack, T. Okada, P. Soós, R. Istók, T. Radovits, B. Straub, E. Barnucz, S. Loganathan, I. Pätzold, N. Chaimow, C. Schies, S. Korkmaz, U. Tochtermann, M. Karck, G. Szabó, Reendothelialization of human heart valve neoscaffolds using umbilical cord-derived endothelial cells, Circ. J. 77 (2013) 207–216, https://doi.org/10.1253/circj.CJ-12-0540.
[39] N. Côté, P. Pibarot, M.A. Clavel, Aortic stenosis: what is the role of aging processes? Aging 11 (2019) https://doi.org/10.18632/aging.101826.
[40] C.E. Roată, Ştefan Iacob, Ştefan Morărașu, C. Livadaru, I. Tudorancea, S. Luncă, M.G. Dimofte, Collagen-binding nanoparticles: a scoping review of methods and outcomes, Crystals 11 (2021), https://doi.org/10.3390/cryst11111396.
[41] R. Molinaro, M. Yu, G. Sausen, C.A. Bichsel, C. Corbo, E.J. Folco, G.Y. Lee, Y. Liu, Y. Tesmenitsky, E. Shvartz, G.K. Sukhova, F. Kloss, K.J. Croce, O.C. Farokhzad, J. Shi, P. Libby, Targeted delivery of protein arginine deiminase-4 inhibitors to limit arterial intimal NETosis and preserve endothelial integrity, Cardiovasc. Res. 117 (2021), https://doi.org/10.1093/cvr/cvab074.
[42] N. Kamaly, G. Fredman, M. Subramanian, S. Gadde, A. Pesic, L. Cheung, Z.A. Fayad, R. Langer, I. Tabas, O. Cameron Farokhzad, Development and in vivo efficacy of targeted polymeric inflammation-resolving nanoparticles, Proc. Natl. Acad. Sci. USA 110 (2013) 6506–6511, https://doi.org/10.1073/pnas.1303377110.
[43] B. Ganss, R.H. Kim, J. Sodek, Bone Sialoprotein, Crit. Rev. Oral Biol. Med. 10 (1999) 79–98, https://doi.org/10.1177/10454411990100010401.
[44] G. Fredman, N. Kamaly, S. Spolitu, J. Milton, D. Ghorpade, R. Chiasson, G. Kuriakose, M. Perretti, O. Farokhzad, I. Tabas, Targeted nanoparticles containing the proresolving peptide Ac2-26 protect against advanced atherosclerosis in hypercholesterolemic mice, Sci. Transl. Med. 7 (2015), https://doi.org/10.1126/scitranslmed.aaa1065.
[45] N. Kamaly, G. Fredman, J.J.R. Fojas, M. Subramanian, W.I. Choi, K. Zepeda, C. Vilos, M. Yu, S. Gadde, J. Wu, J. Milton, R. Carvalho Leitao, L. Rosa Fernandes, M. Hasan, H. Gao, V. Nguyen, J. Harris, I. Tabas, O.C. Farokhzad, Targeted interleukin-10 nanotherapeutics developed with a microfluidic chip enhance resolution of inflammation in advanced atherosclerosis, ACS Nano 10 (2016) 5280–5292, https://doi.org/10.1021/acsnano.6b01114.
[46] C.A. Constantinescu, E.V. Fuior, D. Rebleanu, M. Deleanu, V. Simion, G. Voicu, V. Escriou, I. Manduteanu, M. Simionescu, M. Calin, Targeted transfection using PEGylated cationic liposomes directed towards P-selectin increases siRNA delivery into activated endothelial cells, Pharmaceutics 11 (2019) 47, https://doi.org/10.3390/pharmaceutics11010047.
[47] D.H. Madsen, S. Ingvarsen, H.J. Jürgensen, M.C. Melander, L. Kjøller, A. Moyer, C. Honoré, C.A. Madsen, P. Garred, S. Burgdorf, T.H. Bugge, N. Behrendt, L.H. Engelholm, The non-phagocytic route of collagen uptake: a distinct degradation pathway, J. Biol. Chem. (2011) 286, https://doi.org/10.1074/jbc.M110.208033.
[48] H. Yang, Y. Song, J. Chen, Z. Pang, N. Zhang, J. Cao, Q. Wang, Q. Li, F. Zhang, Y. Dai, C. Li, Z. Huang, J. Qian, J. Ge, Platelet membrane-coated nanoparticles target sclerotic aortic valves in ape−/− mice by multiple binding mechanisms under pathological shear stress, Int. J. Nanomed. 15 (2020), https://doi.org/10.2147/IJN.S224024.
[49] C.L. Meisel, P. Bainbridge, D. Mitsouras, J.Y. Wong, Targeted nanoparticle binding to hydroxyapatite in a high serum environment for early detection of heart disease, ACS Appl. Nano Mater. 1 (2018), https://doi.org/10.1021/acsanm.8b01099.
[50] C.L. Meisel, Superparamagnetic Iron Oxide Nanoparticles for Early Detection of Calcific Aortic Valve Disease, 2019. https://open.bu.edu/handle/2144/36123.
[51] E.A. Waters, J. Chen, J.S. Allen, H. Zhang, G.M. Lanza, S.A. Wickline, Detection and quantification of angiogenesis in experimental valve disease with integrin-targeted nanoparticles and 19-fluorine MRI/MRS, J. Cardiovasc. Magn. Reson. 10 (2008), https://doi.org/10.1186/1532-429X-10-43.